SLAC-PUB-5798
April, 1992
(T/E)

Physics Issues for the Next Linear Collider

MICHAEL E. PESKIN*

Stanford Linear Accelerator Center
Stanford University, Stanford, California 94309

ABSTRACT

This article surveys the physics issues to be studied at future e^+e^- colliders, especially in the energy region below 500 GeV. Particular emphasis is given to exotic standard model studies—precision measurements of the dynamical properties of W bosons and top quarks—as well as to the search for evidence of the Higgs sector.

1. Introduction

Why should we continue the study of e^+e^- annihilation at higher energies? The experience of the past twenty years, from SPEAR to LEP, has made clear that the experimental environment of e^+e^- annihilation provides an ideal hunting-ground for new particles beyond the standard model. The event structure is relatively simple, the standard model backgrounds are small, and the particle production rates, though low, are democratic between hadrons and leptons, and between familiar and novel particles. As we contemplate the next step in energy, however, there is another motivation: the opportunity to conduct detailed studies of the last and most mysterious objects within the standard model—the W, the top quark, and the Higgs boson. For the study of these particles, all of the previously mentioned advantages of e^+e^- annihilation come into play, along with two more, the availability of precise theoretical predictions for the properties of these particles and the ease of experimental reconstruction of W and Z bosons.

In this article, I will survey the physics issues to be addressed at this next-generation machine, a linear collider with center-of-mass energy 500 GeV. My emphasis will be on the theoretical basis for the various experiments that this collider will carry out and the conceptual questions that these experiments should answer. This discussion will provide an introduction to the later articles of this volume, which will describe these experiments more carefully and estimate, by detailed simulations, the accuracies which can be obtained. Earlier reviews of the physics of e^+e^- linear colliders, which mainly emphasize the physics topics at TeV energies, may be found

* Work supported by the Department of Energy, contract DE-AC03-76SF00515.

Presented at the International Workshop on Physics and Experiments with Linear Colliders, Saariselka, Finland, September 9-14, 1991

in Refs. 1–8.

In the remainder of this section, I will set the stage for this discussion, by outlining the experimental facilities that a next-generation linear collider (henceforth, 'NLC') should make available. I will also offer some questions that machine and detector designers should keep in mind through the more theoretical discussion. In Sections 2–5 I will discuss the features of Higgs boson, W, and top quark production at the NLC and describe how experiments can probe these systems. In Section 6, I will briefly describe some aspects of searches for new particles and interactions at the NLC which are also relevant to the planning for this machine.

1.1 A Wish-List of Facilities

A basic definition of the NLC is an e^+e^- collider which will operate at a center-of-mass energy of 500 GeV, with a luminosity of order 10^{33} cm^{-2}sec^{-1}. In e^+e^- annihilation, the size of cross sections is normally some multiple of the QED cross section for $e^+e^- \to \mu^+\mu^-$:

$$1 \text{ R} = \frac{4\pi\alpha^2}{3s} = \frac{87 \text{ fb}}{E_{\rm CM}^2}, \tag{1}$$

with the center-of-mass energy in TeV. Thus, it is convenient to convert the luminosity to the units of annihilation events for a process with a cross section of 1 R over a hypothetical year of 10^7 sec. This gives

$$10^{33} \text{ cm}^{-2}\text{sec}^{-1} \cdot \left(\frac{E_{\rm CM}}{500 \text{ GeV}}\right)^2 = 3000 \text{ events/R} \cdot \text{yr}. \tag{2}$$

This luminosity is what is required to provide an event sample comparable in size to that of the PEP and PETRA experiments.

To take full advantage of the energy of the NLC several other features are desirable. First, the energy should be adjustible downward, to explore the threshold region of $t\bar{t}$ production and, possibly, to optimize the search for the Higgs boson. At the end of the article, I will discuss the possibilities opened by probes to higher energies, up to about 2 TeV. Second, the accelerator should allow the use of a polarized electron beam. I will describe several experiments which make essential use of electron polarization. (Polarizing the positron beam as well gives no extra advantages.)

Third, the facility should allow experimenters to collide the electron bunches with a visible-light laser, just before interaction point. This collision can convert the electron beam to a converging, high-energy photon beam, with essentially no loss of luminosity. The possibility of creating a photon collider in this way was raised ten years ago in a beautiful series of papers by Ginzburg, Kotkin, Panfil, Serbo, and

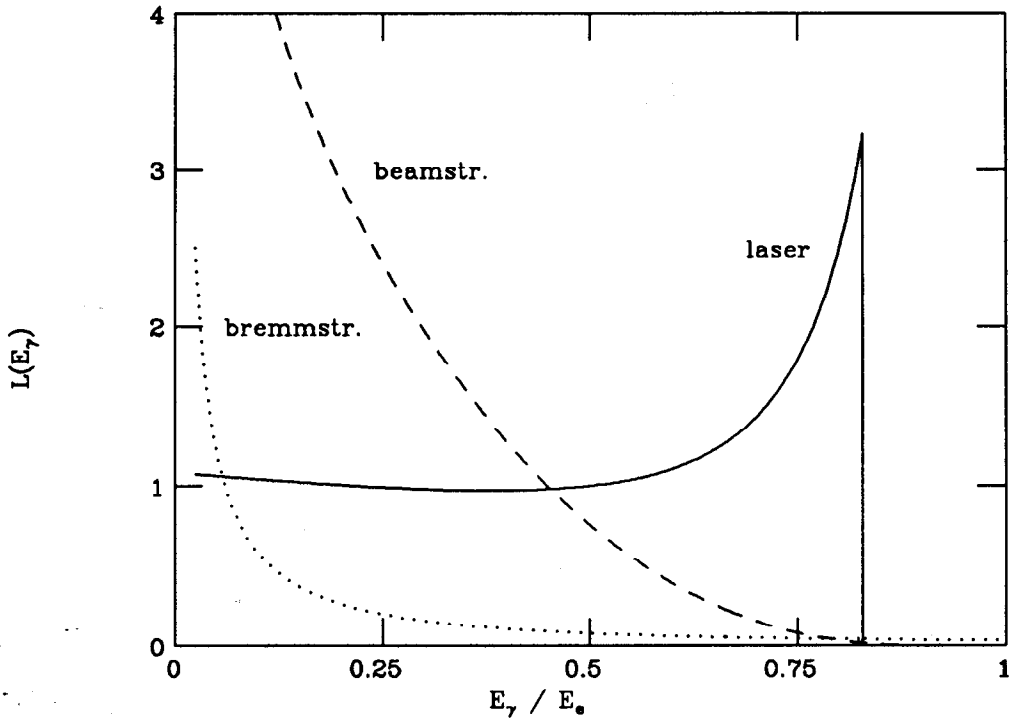

Figure 1. Comparison of photon spectra from bremmstrahlung (Weizsacker-Williams distribution), beamstrahlung (computed for the Palmer G 500 GeV e^+e^- collider[11]), and the backscattered laser technique, from Ref. 12.

Telnov.[9,10] This group made a detailed analysis of the polarization-dependence of the scattering process and emphasized that one can use the polarization of the laser and the electron beam both to polarize the final photon beam and to sharpen its energy dependence. Even without polarization, the photon spectrum from the backscattered laser technique is remarkably weighted toward high energies. Conventional two-photon physics uses a photon beam created as a byproduct of e^+e^- reactions; the typical photon energy is much lower than that of the electron beam. In contrast, even without the use of the polarization effect, the backscattered laser technique produces a spectrum of photons comparable in energy to that of the original electron beam; this comparison is shown in Fig. 1. The backscattered laser technique thus makes it interesting to contemplate high-energy $e\gamma$ and $\gamma\gamma$ experiments in addition to e^+e^- (and e^-e^-) collision processes. Of these new reactions, the $\gamma\gamma$ collision process is the most interesting and will play a role at several points in my discussion.

1.2 Questions for Experimenters and Machine Designers

At the same time that we plan the experimental facilities which the NLC will make available, it is important also to consider the requirements that the physics goals impose on the experimental environment, both in the accelerator and in the detector design. These issues are still being explored and, in any event, cannot be dealt with in the space of this review. However, I would like to highlight the most important issues of this type, so that these might be kept in mind as we discuss specific experiments.

The designer of an e^+e^- collider begins with a machine which naturally provides a very clean experimental environment and, at the same time, a very low event rate. To increase the event rate, one must contemplate extremely tightly focussed and dense electron and positron bunches. This affects the cleanliness of experiments, in several stages. First, there may be backgrounds from production of electrons, photons, and muons upstream of the collision point. Second, during the collision process, the electrons may emit synchrotron radiation in the electromagnetic field of the positron bunch, and vice versa. For realistic designs, this radiation, called 'beamstrahlung', approaches the quantum regime where a single photon carries off a signficant fraction of its parent electron's energy.[13] Third, the photons may then convert to e^+e^- pairs, raising the possibility that one member of each pair may be ejected from the bunch into the detector.[14] Finally, the beamstrahlung photons may interact to produce hadrons, which appears as extra tracks in some fraction of the e^+e^- annihilation events.[15]

For e^+e^- collisions energies up to 500 GeV, there exist reasonable designs for which only a few percent of events contain significant beamstrahlung radiation, with the machine luminosity still kept above 10^{33} cm^{-2}sec^{-1}.[11] At higher energies, though, it appears that one must accept significant beamstrahlung and the associated backgrounds. These processes affect experimentation in several ways: They smear out the precisely defined center-of-mass energy of annihilation. They make it difficult to detect particles at small angles, typically, within 10° of the beam direction. They also may create backgrounds for precision vertex detectors, which one would ideally like to place within millimeters of the interaction point. In the worst scenarios envisioned in Ref. 15, they provide an underlying hadronic event reminiscent of the proton fragments in hadron colliders. None of these phenomena compromise the most essential features of e^+e^- experimentation, the simplicity of events and the democracy among produced species. But these and similar background may nevertheless limit the luminosity of a linear collider.

Studies of these backgrounds are necessarily tied to the physics goals of the experiments; precision studies of specific reactions should be more sensitive to energy smearing, for example, than broad-band searches for new particles. It is fortunate, in

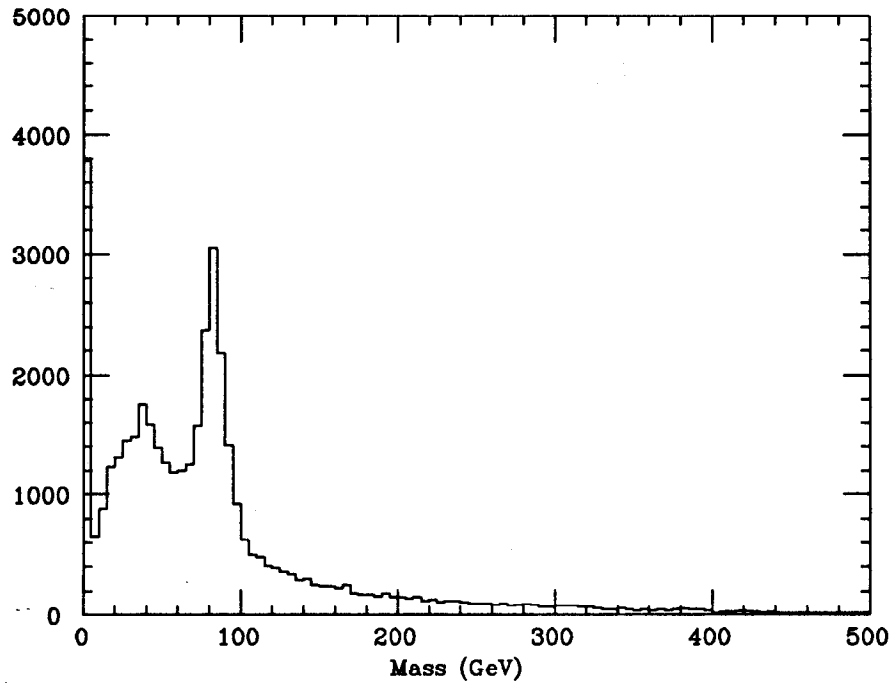

Figure 2. Distribution of the calorimetrically reconstructed mass in a hemisphere cut perpendicular to the thrust axis, for e^+e^- annihilation events at $\sqrt{s} = 1$ TeV, from Ref. 6.

fact, that those experiments which are most sensitive to backgrounds are also those at the lowest energies, where the beamstrahlung problem is easiest to control. However, much more work needs to be done on the detailed effects of these backgrounds. In my discussion of the specific experiments, I will try to indicate directions for further analysis by pointing out places in which definition of the center-of-mass energy, tagging of small-angle particles, and b-tagging with a vertex detector play a crucial role. I will also note one experiment for which the intrinsic energy spread of the machine is a crucial parameter.

In addition to the capabilities of the accelerator, we must also give some thought to the required capabilities of a detector. One of the main points of my theoretical discussion will be that weak vector bosons play a crucial role in most important physical processes at the NLC. It is therefore crucial that the NLC detector be able to reconstruct W bosons as systems of two hadronic jets. The basic advantages of the e^+e^- environment make this a much easier task than at hadron colliders: W bosons

are produced at a rate comparable to that of quark pair production, and the effect of gluon radiation producing high mass jets is quite modest. To give a simple illustration of this point, I reproduce in Fig. 2 a plot from the 1988 SLAC study of the physics of a 1 TeV linear collider.[6] For historical reasons, the authors of this study included a large beamstrahlung energy smearing and performed their analysis with relatively loose cuts on thrust angle and total visible energy. Nevertheless, they found, for the reconstructed invariant mass distribution in a hemisphere, the spectrum of Fig. 2, which shows a clear and quite narrow W mass peak. This analysis demonstrates the promise that one can identify, measure, and track W bosons from the final states of e^+e^- annihilation at the NLC. I will now explain what we expect to learn from this investigation.

2. W and Z Bosons at the NLC

The most successful e^+e^- colliders have been those optimized for the study of a particular particle, for example, c, b, or Z^0. In the same spirit, the NLC is expected to be a factory for top quarks, and may also produce great numbers of some other, as yet undiscovered, species. More generally, though, the NLC will be a factory for producing relativistic W and Z bosons. The direct pair-production cross sections for these particles are large, and they are also produced indirectly in top quarks decays. If exotic particles are present, these are also likely to decay to weak bosons. Before discussing the specific NLC experiments, then, it is useful to review some properties of the W and Z. I would also like to explain why it is particularly interesting that these bosons will be relativistic, that is, why high-energy vector bosons are more interesting than the quiescent variety that we can already study at LEP and LEP II.

2.1 Golstone Boson Equivalence

For a W boson at rest, all polarizations are equivalent. However, for a W boson in relativistic motion, the longitudinal polarization state takes on a special signficance. One might suspect that this state would be particularly interesting, because photons and other massless gauge bosons cannot have a longitudinal polarization. Thus, the properties of this state should be bound up in some way with the mechanism of mass generation for the W boson.

To pose the question more explicitly, consider a W boson at rest, with polarization vector $\epsilon^\mu = (0,0,0,1)$. If this boson is boosted along the $\hat{3}$ axis to energy E and

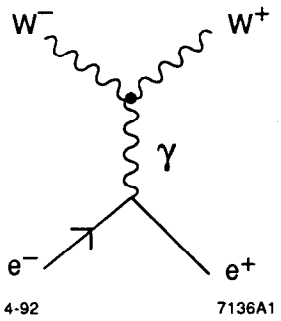

Figure 3. A Feynman diagram contributing to $e^+e^- \to W^+W^-$.

momentum k, the polarization vector boosts to

$$\epsilon^\mu(k) = (\frac{k}{m_W}, 0, 0, \frac{E}{m_W}). \tag{3}$$

The components of the longitudinal polarization vector grow proportionally to the energy.

These large components can actually show up in the evaluation of Feynman diagrams. For example, the diagram shown in Fig. 3 contains (among other terms) the amplitude for scalar pair-production in e^+e^- annihilation times the dot product of the W^+ and W^- polarization vectors. When both W's are longitudinally polarized, this latter factor is

$$\epsilon(k_+) \cdot \epsilon(k_-) \approx \frac{2E^2}{m_W^2} \approx \frac{s}{2m_W^2}. \tag{4}$$

When the amplitude is squared, the s-wave cross section is predicted to rise faster than would be allowed by unitarity by a factor of $(s/m_W^2)^2$.

Such a rapid growth of the cross section is unphysical unless it is halted by some cancelling mechanism. There are two possible sources for this cancellation. Most directly, the growth of the cross section could be cut off by a W boson form factor. In this case, the W bosons would be composite, rather than elementary particles, and their interactions would begin to deviate from those of an elementary vector particle when the factor (4) became large. However, if W bosons are not only elementary but also gauge bosons which receive their mass through the Higgs mechanism, there is another, much more elegant cure: The Ward identity implies a series of cancellations between diagrams which remove all of the dangerous terms. In fact, the Ward identity even predicts the result of this cancellation, a beautiful relation shown in Fig. 4 called the Goldstone Boson Equivalence Theorem.[16–19] This Equivalence Theorem states that a longitudinal W boson emitted at high energy has precisely the interactions of

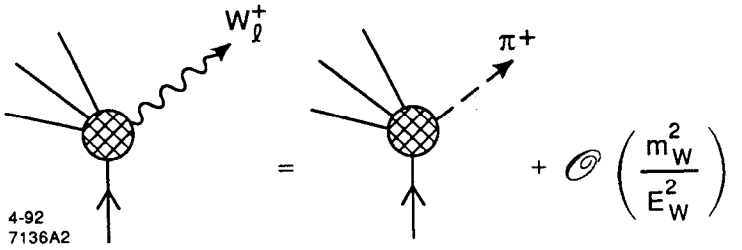

Figure 4. The Goldstone Boson Equivalence Theorem.

the (unphysical) Higgs boson which the W absorbed to become massive. In addition, Cornwall, Levin, and Tiktopoulos showed that there is no middle ground between these two possibilities: An elementary vector boson whose couplings differ from that implied by gauge invariance has interactions which violate unitarity.

Thus, as soon as we enter a regime in which we produce relativistic W bosons, the simplest experimental observations of the W properties will demonstrate one of two remarkable possibilities. Either the W bosons will be manifestly composite particles, with a detailed pattern of discrepancies from the standard model, or they will be a window into the mysterious Higgs sector. Either option would be well worth exploring.

2.2 A Primer of W Physics

Let us now review some properties of the W and Z bosons which will play a role in the NLC experiments. I begin with the W.

In the standard model, the W boson is expected to decay 67% of the time to hadrons, and 11% of the time to each lepton and its associated neutrino. The hadronic decays are essentially equally divided between the $u\bar{d}$ and $c\bar{s}$ modes, with Cabibbo mixing. Bottom quarks should appear only through the mode $W \to c\bar{b}$, which has a branching ratio of 0.1%, due to a small CKM matrix element. For events with two W bosons, this implies the following branching ratios:

$W^+ \to$ hadrons	$W^- \to$ hadrons	45%
$W \to$ hadrons	$W \to (e$ or $\mu)\ \nu$	29%
$W^+ \to (e$ or $\mu)\nu$	$W^- \to (e$ or $\mu)\ \nu$	5%

If τ leptons can also be used effectively to reconstruct W's, the useful semileptonic and purely leptonic fractions go up to 44% and 11%, respectively.

The standard model also makes precise predictions for the W decay distribution.

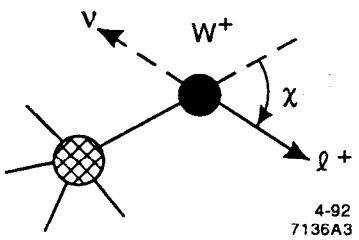

Figure 5. Definition of the W boson decay angle χ.

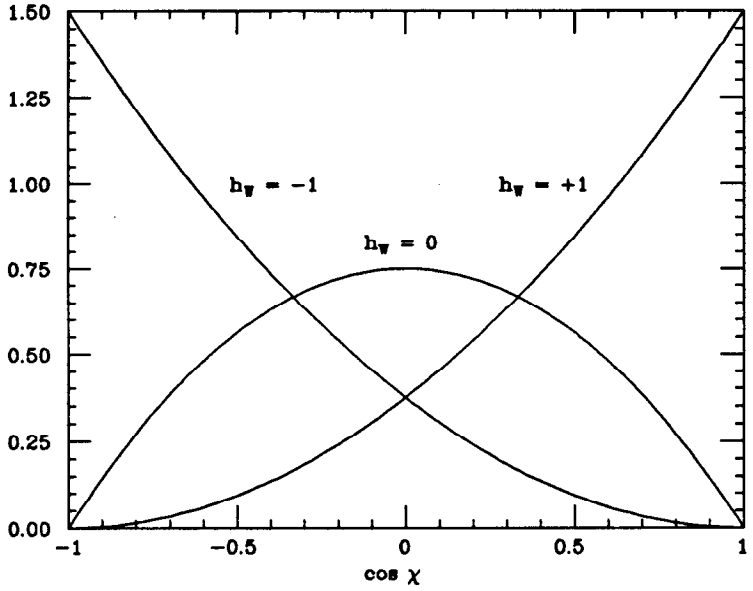

Figure 6. Distributions in χ for the three possible values of W helicity.

At several points in this article, I will make reference to particle pair-production and decay angles. I will try to consistently refer to the production angle as θ; this is defined as the angle between the particle momentum and the electron beam direction, measured in the e^+e^- center-of-mass frame. A decay angle χ will be defined as the angle between the momentum of the decay product and the momentum of the decaying particle, measured after the decaying particle has been boosted to rest. For the case of the W^+, I define χ as the angle between the ℓ^+ momentum and the (original) W^+ momentum, measured in the W^+ rest frame. This angle is indicated in Fig. 5. Because the ν and ℓ^+ emitted in a W^+ decay are always, respectively, left- and right-handed, the decay products form a spin-1 system whose orientation is correlated with the W^+ spin or helicity. More explicitly, the standard model predicts,

for the various possible values of the W^+ helicity, the following distributions:

$$\frac{1}{\Gamma}\frac{d\Gamma}{d\cos\chi} = \begin{cases} \frac{3}{8}(1+\cos\chi)^2 & h_W = +1 \\ \frac{3}{4}\sin^2\chi & h_W = 0 \\ \frac{3}{8}(1-\cos\chi)^2 & h_W = -1. \end{cases} \tag{5}$$

The three distributions are shown in Fig. 6.

Events in which one W decays hadronically and the other decays leptonically provide a particularly powerful setting for the measurement of the production and decay angles. The hadronic W may be constrained to the W mass to define the kinematics of the reaction. The charge of the lepton gives the charge of the leptonic W and thus the sign of the production angle $\cos\theta$; the lepton also indicates the sign of $\cos\chi$. In events for which both W's decay hadronically, the absolute values of both cosines can still be reconstructed. This allows one to determine the most interesting part of the W helicity information, the relative production of longitudinally to transversely polarized W's.

2.3 A Primer of Z Physics

The main difficulty with studying Z physics at the NLC is not that the Z is particularly difficult to detect but rather that it is difficult to separate from the large background of W's. As an illustration, the ratio of Z to W couplings to the left-handed electron is:

$$\left|\frac{e}{\sin\theta_w\cos\theta_w}(\frac{1}{2}-\sin^2\theta_w)\right|^2 \Big/ \left|\frac{e}{\sqrt{2}\sin\theta_w}\right|^2 \sim 0.2. \tag{6}$$

Thus, it is difficult to separate Z bosons from W's on the basis of their mass alone, even if the peaks of their mass distributions can be separated by several σ.

It is therefore important to make use of the characteristic decay modes of the Z which cannot be confused with W decays. The most important of these are:

$Z^0 \to e^+e^-$ or $\mu^+\mu^-$	7%
$Z^0 \to \tau^+\tau^-$	3%
$Z^0 \to \nu\bar{\nu}$	20%
$Z^0 \to b\bar{b}$	15%

The leptonic decay modes of the Z are the most well-known of these characteristic modes, but they are relatively rare. The $\nu\bar{\nu}$ decay mode is most effective in events of

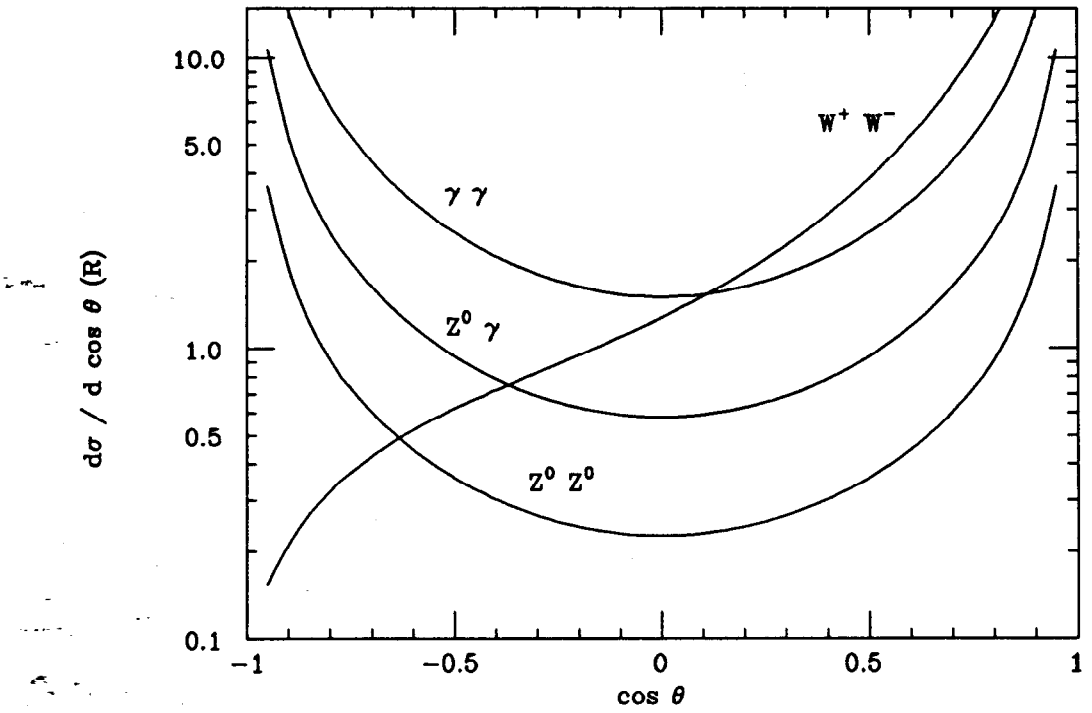

Figure 7. Differential cross sections for two gauge boson production processes in e^+e^- annihilation at $\sqrt{s} = 500$ GeV.

very simple topology in which the Z can be reconstructed from missing momentum. This mode has been used effectively in the Higgs boson search at LEP and should also be useful at the NLC. The most effective mode, however, should be the $b\bar{b}$ mode, which can be identified with high efficiency in a precision vertex detector. Since W bosons hardly ever decay to b quarks, the b vertex is a powerful marker of a Z. In Z pair production (for example, $e^+e^- \to Z^0Z^0$), 44% of the events have a Z which decays either to leptons or to $b\bar{b}$. This fraction goes up to 70% if the neutrino modes are included.

The production cross sections for gauge boson pairs at the NLC are of order units of R, comparable to the cross section for $e^+e^- \to \gamma\gamma$ at more familiar energies. The production cross sections are shown as a function of $\cos\theta$ in Fig. 7.

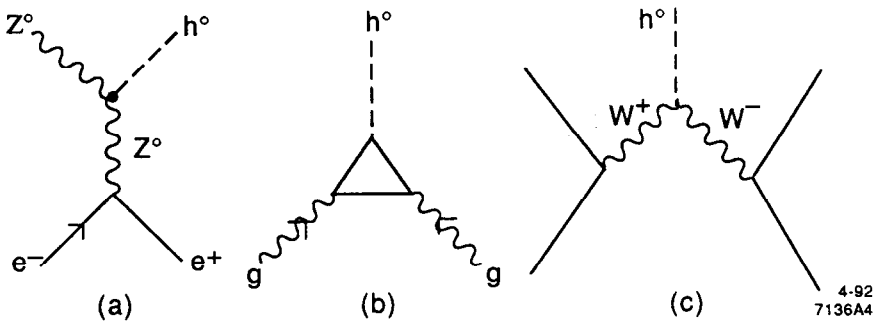

Figure 8. Processes which produce the Higgs boson: (a) $e^+e^- \to h^0Z^0$; (b) gluon-gluon fusion; (c) W^+W^- fusion.

3. Low-Mass Higgs Bosons

With this introduction, we can begin our discussion of the experiments to be carried out at the NLC. I will mainly emphasize precision measurements within the standard model. However, it will be instructive to begin with an experiment which is just slightly speculative: the search for a low-mass Higgs boson. In this section, I will concentrate on the search for the single Higgs scalar h of the minimal standard model. More general models are possible, and even likely. In fact, if a Higgs scalar is found, it will be important to probe its couplings in as many ways as possible to see if it fits the predictions of the minimal model. We will see that, once the Higgs boson is found, it can be studied in a variety of ways at the NLC.

3.1 Prospects for Discovery of the Higgs Boson

Searches for the Higgs boson have been discussed by many authors in the past few years, both because the search for the Higgs has been an important topic in the LEP experimental program and because this search has been an important motivation for the construction of the high-energy proton colliders SSC and LHC. The theoretical analysis is usefully summarized in the book of Gunion, Haber, Kane, and Dawson.[20] Here, I will review a few features of their discussion which are relevant for understanding the role of the NLC.

As of the summer of 1991, the standard model Higgs boson had been searched for in Z^0-decays and excluded up to a mass of 57 GeV.[21] Some further progress can be made by increasing the Z^0 event sample at LEP. When the energy of LEP is raised to 180 GeV, it will be possible to search for the Higgs boson in a larger mass region, up to about 85 GeV, using the process $e^+e^- \to h^0Z^0$, shown in Fig. 8(a).[22] The precise

range available depends upon the eventual maximum energy of LEP II, but probably it will be difficult to extend this search to Higgs masses above the Z^0 mass.

One of the main attractions of the proton supercolliders is that they will be able to search for the Higgs boson up to very high energies. The standard Higgs boson is produced copiously in proton colliders by the reactions of gluon and W boson fusion (Fig. 8(b) and (c)). If the Higgs boson is sufficiently heavy, it decays dominantly to weak boson pairs W^+W^- and Z^0Z^0. The Z^0Z^0 decay is readily observed even in the environment of hadron colliders, and methods have been proposed to observed the W^+W^- channel also.[23] This search is very powerful for Higgs bosons in the mass range 160–700 GeV, but it is less effective outside this range. If the mass of the Higgs boson is below $2m_Z$, one of these vector bosons must be virtual, and the rate for producing the Z^0Z^0 final states decreases, dropping to tens of events per SSC year for Higgs masses below 130 GeV. As explained in Ref. 20, a lower-mass Higgs boson can be discovered by reconstructing its decay $h^0 \to \gamma\gamma$. In either case, the hadron collider gives only a narrow window onto the properties of this new state. At the other extreme, if the Higgs boson is very heavy, it becomes a broad resonance which is increasingly difficult to recognize above background.

Unfortunately, these two cases, in which the mass of the Higgs boson is either extremely low or extremely high, are the cases which are most likely from theoretical considerations. If the Higgs boson is weakly coupled, its mass is also small compared to the mass scale set by the Higgs vacuum expectation value

$$v \equiv \langle \phi \rangle = 250 \text{ GeV}. \tag{7}$$

Renormalization effects cause the Higgs self-coupling to increase at high energies. Thus, if there is a grand unification, and if the Higgs boson has any moderate value of its self-coupling at this scale, it will be weakly coupled and light at weak-interaction energies. Fig. 9, taken from Ref. 20, shows the effect of this restriction. In grand unified models with a larger Higgs structure, it is generally true that at least one Higgs boson obeys a similar bound. The specific case of supersymmetry will be discussed in Section 6.1. On the other hand, if there is no grand unification, it is most likely that the Higgs boson is a composite state, with strong interactions. In that case, its mass will be pushed to the upper end of its allowed range, to 1 TeV and above.

Thus, the two extreme cases of a light and a heavy Higgs boson have a special interest. In the rest of this section, I will concentrate on the case of the light Higgs boson. I will discuss the question of Higgs boson strong interactions in Section 6.2.

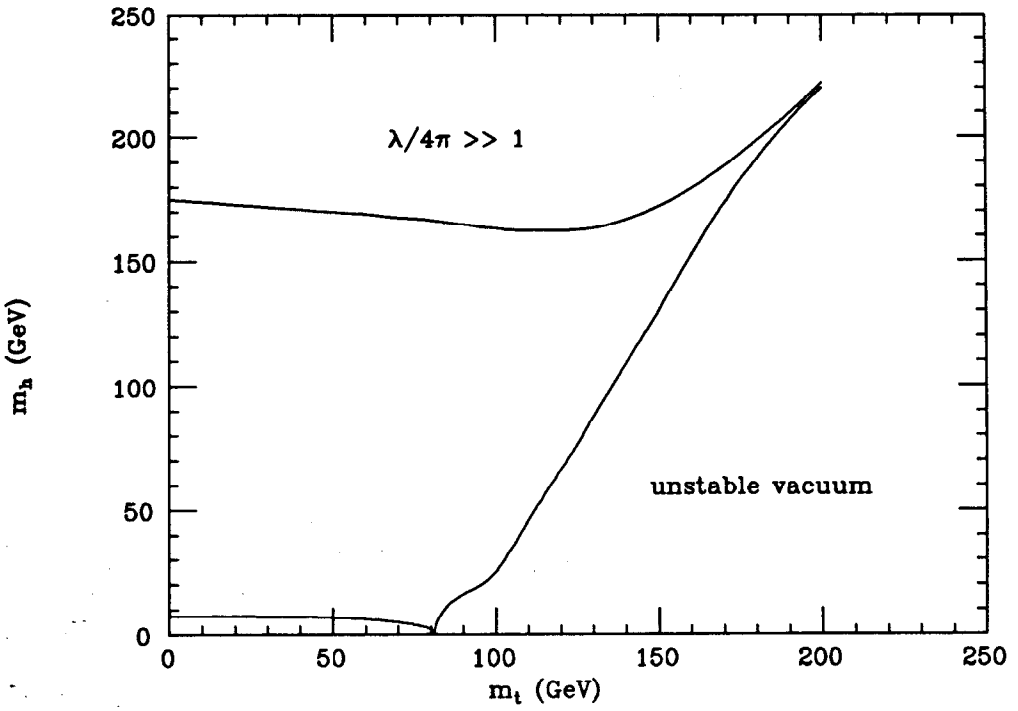

Figure 9. Limits on the mass of the Higgs boson in the minimal standard model, based on the compatibility with grand unification at a scale above 10^{16} GeV. The figure is taken from Ref. 20, whose analysis is in turn based on the work of Cabibbo, Maiani, Parisi, and Petronzio.[24]

3.2 The Higgs Boson in e^+e^- Annihilation

To produce a light Higgs boson in e^+e^- annhilation, one might make use of the reaction of Fig. 8(a) or the leptonic analogues of the reactions in Fig. 8(b) and (c): $\gamma\gamma$ fusion or W^+W^- fusion with the bosons radiated from the initial electron and positron. For an e^+e^- collider with center-of-mass energy below 500 GeV, the small phase space for W radiation and the soft spectrum of γ radiation make these last two reactions less suitable. In addition, one must worry about backgrounds from the two-photon process for reactions whose visible products have a mass much less than the full energy of the e^+e^- collision. Thus, I will concentrate my attention on the process $e^+e^- \to Z^0h^0$.

The process of Higgs production associated with a Z^0 has a relatively small cross section, roughly 0.1 R. However, its detailed distributions have several features which

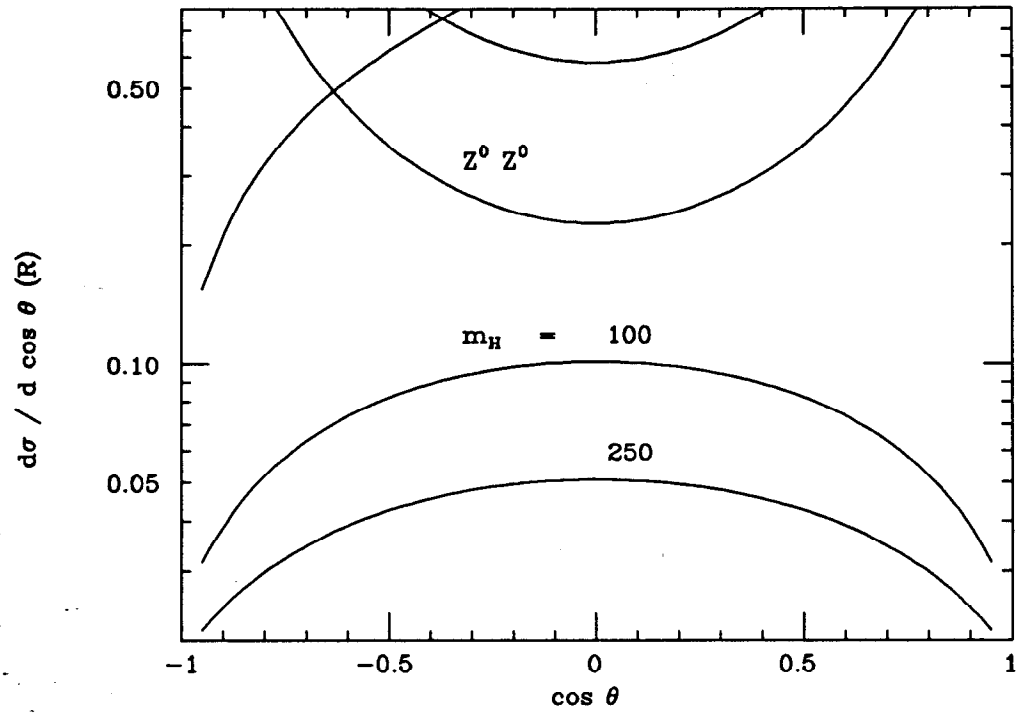

Figure 10. Differential cross section for $e^+e^- \to h^0Z^0$ at $\sqrt{s} = 500$ GeV, compared to the cross sections for two gauge boson production displayed in Fig. 7.

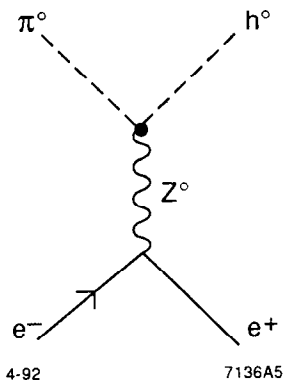

Figure 11. The process $e^+e^- \to h^0\pi^0$, which determines the properties of $e^+e^- \to h^0Z^0$ at high energies through Goldstone boson equivalence.

are characteristic of its Higgs origin. The differential cross section is plotted in Fig. 10 and compared to the cross section for $e^+e^- \to Z^0Z^0$. If p is the final-state momentum and $y = 2p/\sqrt{s}$, we can write the explicit form of this distribution as

$$\frac{d\sigma}{d\cos\theta} = \frac{1}{16}\left[\frac{(\frac{1}{2} - \sin^2\theta_w)^2 + (\sin^2\theta_w)^2}{2\sin^4\theta_w\cos^4\theta_w}\right]\frac{1}{(1-m_Z^2/s)^2}\cdot\left(\frac{3}{4}y^3\sin^2\theta + 6y\frac{m_Z^2}{s}\right), \quad (8)$$

in units of R. The angular factor $\sin^2\theta$ in the last term is the signal of e^+e^- annihilation into a pair of scalars, and indeed the cross section for $s >> m_Z$ matches that for the process shown in Fig. 11, in which the Higgs is produced in association with a neutral Goldstone boson. This is just the prediction of the Equivalence Theorem. A corollary of this result is that the Z^0 is dominantly longitudinally polarized, in contrast to the dominantly transverse polarization predicted for $e^+e^- \to Z^0Z^0$. Thus, the measurement of $\cos\chi$ (or even its absolute value) in the Z^0 decay can aid in distinguishing this process from Z^0 pair production.

Once the Higgs boson has been found and its mass measured, it is important to test the couplings of the Higgs boson to fermions of each type by measuring the Higgs branching ratios. The minimal standard model makes definite predictions for the branching ratios to the various fermion species, and these predictions are the first phenomena upset if the Higgs structure is generalized. From the event rates expected for the NLC, any branching ratios of the h^0 above 1% are interesting targets for verification. For a Higgs mass of 100 GeV, in the minimal standard model, the dominant branching ratios are:

$\mathrm{BR}(h^0 \to b\bar{b})$	$\approx$	90%
$\mathrm{BR}(h^0 \to c\bar{c})$	$\approx$	5%
$\mathrm{BR}(h^0 \to \tau^+\tau^-)$	$\approx$	4%
$\mathrm{BR}(h^0 \to gg)$	$\approx$	2%

The first three of these modes should be straightforward to observe with a precision vertex detector. It would be wonderful to measure the branching ratio to two gluons (which gives the dominant decay of the h^0 to final states without heavy fermions), but I do not know a useful signature of this decay.

3.3 The Higgs Boson in $\gamma\gamma$ Annihilation

The Higgs boson coupling to two photons can also be measured at the NLC, by using the inverse process $\gamma\gamma \to h^0$ and the idea presented in Section 1.1 that the NLC may be converted to use as a a photon-photon collider. The measurement is a particularly interesting one, since the coupling of the Higgs boson to two photons is a loop effect and thus depends on a sum rule over all heavy charged species.[25] If the

mass of the photon-photon final state can be determined to within a resolution Δm, the observable cross section for Higgs production is

$$\frac{1}{\Delta m}\int dm\,\sigma(\gamma\gamma\to h^0) = \frac{4\pi^2}{m_\phi^2}\cdot\frac{\Gamma(h^0\to\gamma\gamma)}{\Delta m} \sim(3\times 10^{-2})\cdot\left(\frac{10\ \text{GeV}}{\Delta m}\right), \tag{9}$$

in units of R. This result is to be contrasted with the cross sections of 9×10^{-2} R for continuum $b\bar{b}$ production and 150×10^{-2} R for continuum $c\bar{c}$ production. However, these backgrounds can be controlled by varying the relative photon polarization. The Higgs is produced only when the photon spins are antiparallel, to form a spin-zero state. However, helicity conservation prohibits the pair-production of massless fermions from this polarization state. This polarization effect can give the factor of 5 suppression of the $b\bar{b}$ channel necessary to bring the Higgs signal into focus.[10]

4. W Couplings and Dynamics

From the minor, but very interesting, reaction of Higgs boson production, we now turn to the most important single process in high-energy e^+e^- annihilation, W boson pair production. The ease of reconstructing W bosons at the NLC allows this process to be studied in great detail, to reveal, for example, the correlation of W polarizations with the production angle. The standard model predictions for W pair production are already quite complex, and this complexity lends a certain richness to the search for anomalies in the W events.

4.1 The Question of W Anomalous Couplings

Why is it important to verify the standard model prediction for W pair production in e^+e^- annihilation? The question is a fundamental one which goes to the heart of the gauge-theory construction of the standard model. The central idea of Yang-Mills theory is that symmetry principles uniquely determine the interactions of vector bosons. The process $e^+e^-\to W^+W^-$ is the ideal place to make a precision test of this idea.

An important ingredient in the amplitude for $e^+e^-\to W^+W^-$ is the γW^+W^- vertex, for which the standard model makes a precise predition: If the vertex is defined as in Fig. 12, and the W bosons are on shell, then we should find:

$$i\Gamma^{\alpha\beta\mu}(p,q,\bar{q}) = -ie\left[g^{\alpha\beta}(q-\bar{q})^\mu + 2(g^{\mu\beta}p^\alpha - g^{\mu\alpha}p^\beta)\right]. \tag{10}$$

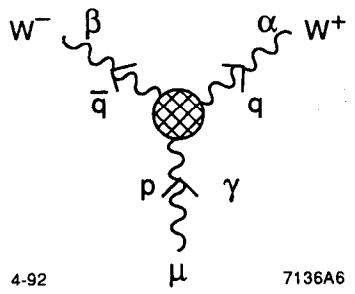

Figure 12. Kinematics of the $W^+W^-\gamma$ vertex.

The first term follows from the fact that the electric charge of the W is 1; the second term implies that the magnetic moment is given by $g = 2$.

In principle, one might find a more general collection of terms. The most general CP-conserving $WW\gamma$ vertex includes, in addition to the terms in (10), arbitrary modifications of the magnetic dipole and electric quadrupole moments of the W, as well as a parity-violating term:

$$i\Delta\Gamma^{\alpha\beta\mu}(p,q,\overline{q}) = -ie\big[(\kappa{-}1+\lambda)(g^{\mu\beta}p^{\alpha} - g^{\mu\alpha}p^{\beta}) - \lambda\frac{1}{m_W^2}p^{\alpha}p^{\beta}(q-\overline{q})^{\mu} + ig_5\epsilon^{\mu\alpha\beta\gamma}(q-\overline{q})_{\gamma}\big]. \tag{11}$$

Such modifications are expected in models in which the W boson is composite and $SU(2)\times U(1)$ is not a true gauge symmetry. They are also expected in gauge-invariant models in which the vector bosons are dynamically generated or simply coupled to a strongly interacting sector.[26–28] The coupling g_5 is omitted in most discussions in the literature, and I will follow that practice in this review.

It should be emphasized, though, that even if the W vertex is modified as in (11), these modifications need not be large. Claudson, Farhi, and Jaffe[29] have argued in models with composite W bosons that the corrections to the W vertex are naturally of order

$$(\kappa - 1),\ \lambda,\ \sim (\frac{m_W}{M}), \tag{12}$$

where M is the mass of the first excited state with the quantum numbers of the W. This means that the natural size of the parameters of anomalous W interactions might be as small as a few percent. A similar order-of-magnitude estimate follows from the consideration that the anomalous W interactions not produce corrections to the observables measured with precision at LEP.

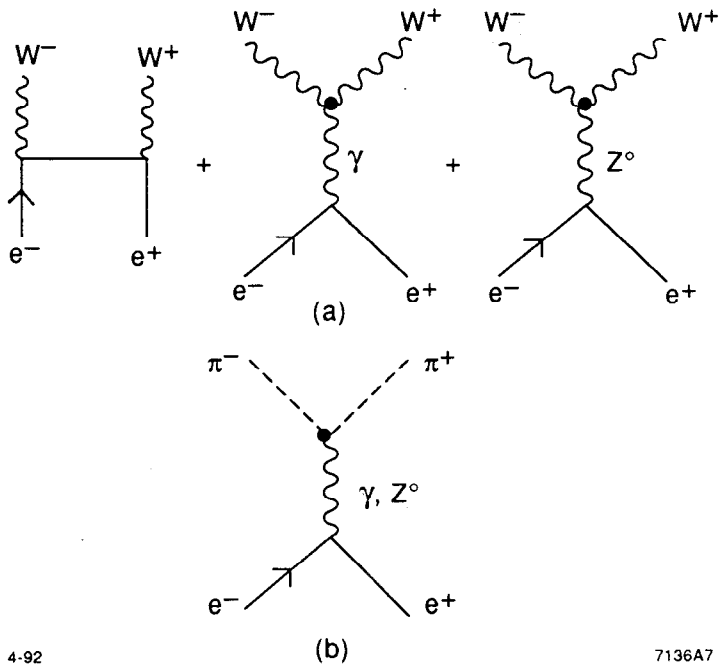

Figure 13. (a) Leading-order diagrams for $e^+e^- \to W^+W^-$; (b) the process $e^+e^- \to \pi^+\pi^-$, related to the pair-production of longitudinal W bosons by Goldstone boson equivalence.

In principle, the W anomalous couplings can be bounded by direct measurements at hadron or lepton colliders. The CDF measurement of the $W\gamma$ production cross-section in $p\bar{p}$ collisions already implies (in a one-parameter analysis) a limit $|\kappa - 1| < 12$.[30] The SSC should eventually improve this limit to a constraint on λ at the 2% level, with less sensitivity to κ.[31] The direct constraints on κ and λ from e^+e^- experiments will begin with the measurement at LEP II of the cross section for $e^+e^- \to W^+W^-$ near threshold. Through this measurement, the LEP experiments will be able to set limits on κ and λ of order 0.1–0.2. In view of the argument in the previous paragraph, this would still be a relatively weak limit. To improve on this limit, we must ask whether one might find improved sensitivity to κ and λ in e^+e^- measurements at higher energies.

4.2 $e^+e^- \to W^+W^-$: Standard Model

In fact, one expects a dramatic improvement in one's sensitivity to anomalies in the W vertex functions with even modest increase in the e^+e^- center-of-mass energy. To understand this statement, we should recall some details of the calculation of $e^+e^- \to W^+W^-$ in the standard model. At tree level, the calculation involves the first diagrams of Fig. 13(a). If the W bosons are transversely polarized, each diagram becomes independent of s at high energy, leading to a differential cross section which varies as $1/s$, *i.e.*, one which is constant in units of R. If the W bosons are longitudinally polarized, we argued in Section 2.1 that the individual Feynman diagrams grow as (s/m_W^2). The Ward identities of the standard model imply that these growing terms cancel between the s- and t-channel diagrams, producing an amplitude which is independent of s. According to the Goldstone Boson Equivalence Theorem, this amplitude should equal that for e^+e^- annihilation into charged Goldstone bosons, as shown in Fig. 13(b). However, the anomalous terms in the $WW\gamma$ and WWZ vertices do not respect this Ward identity. Thus, these anomalous terms are enhanced relative to the standard model by a factor (s/m_W^2). The enhancement with energy is in fact somewhat larger, since the cross section for producing longitudinal W bosons has an extra factor of β^2 near threshold compared to the cross section for producing transversely polarized W's. In all, the effect of anomalous W couplings on the differential cross section for $e^+e^- \to W^+W^-$ is expected to be larger at the NLC than at LEP II by the ratio of factors

$$\beta^2 \cdot \frac{s}{m_W^2}. \tag{13}$$

This corresponds to an increase in sensitivity of a factor 10 from $\sqrt{s} = 200$ GeV to $\sqrt{s} = 400$ and of a factor 15 if one goes up to 500 GeV.

To understand the effect of these anomalous terms, it is useful to first understand the structure of the standard model differential cross section for $e^+e^- \to W^+W^-$. The shape of this cross section is plotted in Fig. 14 for the individual polarization components and for the total rate. Notice that the shape of the cross section for pair-production of longitudinal W bosons is approximately $\sin^2\theta$, as one would expect from the Equivalence Theorem. The variation of the W polarization with the production angle θ is made manifest in the χ distributions shown in Fig. 15. At forward angles, the first diagram in Fig. 13(a) dominates; this diagram dominantly produces a right-handed W^+ and a left-handed W^-, leading to a decay angle distribution of the form $(1 + \cos\chi)^2$. At central and backward angles, the longitudinal W production becomes more important and the component of the decay angle distribution proportional to $\sin^2\chi$ increases.

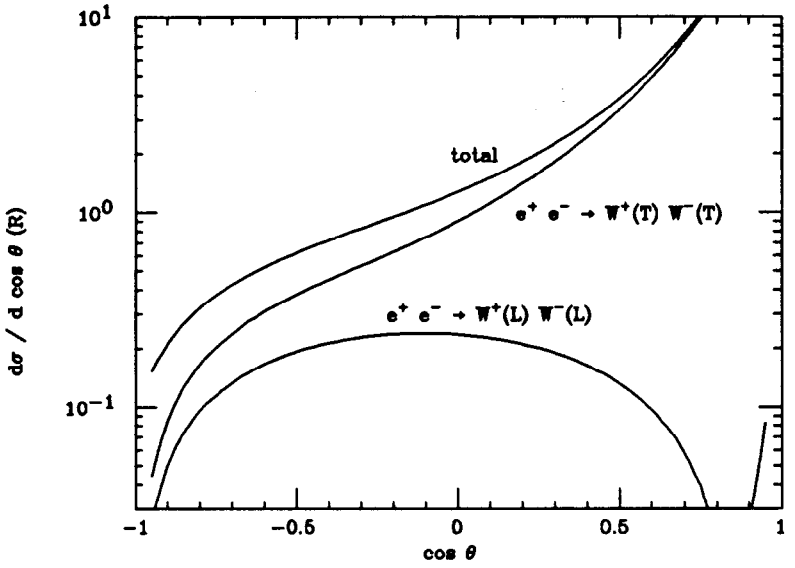

Figure 14. Differential cross section for $e^+e^- \to W^+W^-$, in the standard model, at $\sqrt{s} = 500$ GeV, as a function of the production angle θ. The figure shows also the contribution from transverse and longitudinal W boson pairs.

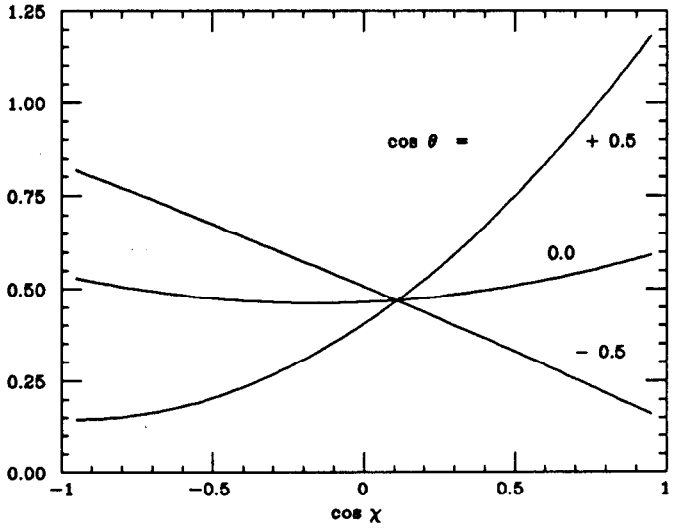

Figure 15. Distributions of $e^+e^- \to W^+W^-$ events in the decay angle χ, for three values of the production angle: $\cos\theta = 0.5, 0.0, -0.5$.

4.3 $e^+e^- \to W^+W^-$: *Anomalies*

It is now easy to imagine how to look for signs of anomalous W interactions. One looks for distortions of the differential cross section in $e^+e^- \to W^+W^-$ especially those associated with an increase in the cross section for pair-production of longitudinally polarized W bosons. The signatures of this effect are easily visualized from Figs. 14 and 15; it induces an increase in the differential cross section at large angles—proportional to $\sin^2\theta$, correlated with an increase in the decay angle distribution at small values of $\cos\chi$. Each available experimental observable gives a complementary piece of information useful in characterizing the anomalous effect.

To understand more quantitatively what constraints the NLC will make available, one must study the detailed form of the cross section as a function of κ, λ, and other anomalous parameters. For the reaction $e^+e^- \to W^+W^-$, this dependence has been worked out in a very useful way by Hagawara, Hikasa, Peccei, and Zeppenfeld.[32]Most recently, several authors have analyzed these formulae from the viewpoint of NLC experimentation.[33,34] In particular, Yehudai has given a simplified but very clear picture of the various complementary constraints.[12]In his analysis, he chose the most characteristic observables which can be extracted from the experimental distributions, assigned each a 3% systematic error (assuming that the standard model gives the central value), and plotted the corresponding 2σ confidence region in the κ, λ plane. For the process $e^+e^- \to W^+W^-$, he considered the effect of measuring the magnitude of the total cross section, the forward-backward asymmetry (FB), the ratio of longitudinal to transverse W production (L/T), and the 'in-out' ratio IO, defined as

$$\mathrm{IO} = \int_{|\cos\theta|<0.4} d\sigma/d\cos\theta \Big/ \int_{|\cos\theta|<0.8} d\sigma/d\cos\theta. \qquad (14)$$

The results of this analysis are shown in Fig. 16. The many independent probes of the process $e^+e^- \to W^+W^-$ available from the NLC complement one another in a most attractive way. The combination of all of these constraints is expected to bound the parameters κ and λ individually at the level of about ± 0.02, up to a two-fold ambiguity. This ambiguity can be resolved by studying the dependence on beam polarization, or, as we will see, by considering other W production processes.

Though a plot such as Fig. 16 is useful for visualization, the various complementary constraints on κ and λ can be taken into account more systematically by a global likelihood analsys. This technique and a discussion of the many experimental issues involved in the measurement of W cross sections are presented in Barklow's article in this volume.[35]

We can obtain an interesting complement to this process by operating the NLC as a $\gamma\gamma$ collider, to study the process $\gamma\gamma \to W^+W^-$. The tree level diagrams are shown

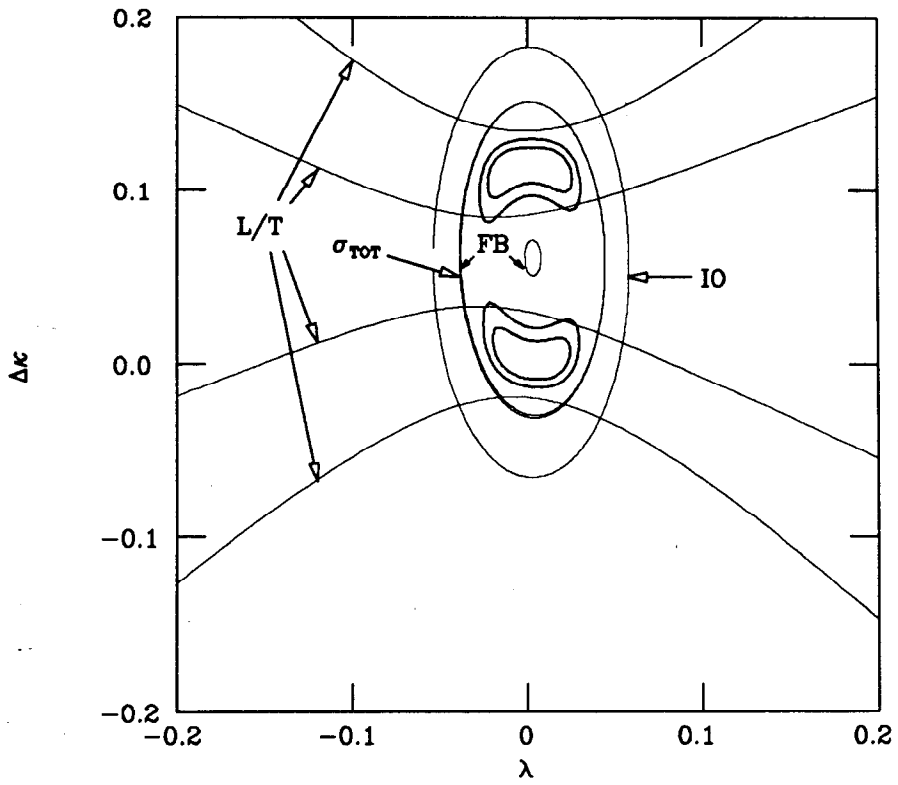

Figure 16. Expected bounds on the parameters κ, λ of the W anomalous couplings expected from the measurement of various features of the cross section for $e^+e^- \to W^+W^-$ at $\sqrt{s} = 500$ GeV, from Ref. 12.

in Fig. 17; these can involve anomalous vertices both in the 3- and 4-weak boson interaction. The sensitivity of the various observable parameters of this cross section to κ and λ has also been studied in Refs. 12, 33, 34. Yehudai's presentation of the determination of κ and λ from this process from the composition of complementary observables is shown in in Fig. 18. In this case, the most sensitive observables, after the total cross section, involve polarization of the photon beam. In the figure, the constraints (0/2) is the ratio of yields for antiparallel as opposed to parallel photon polarization, and $\chi_{\rm FB}$ is the χ forward-backward asymmetry, that is, the ratio of right- to left-handed W^+ bosons emerging from the production process. Notice that the study of the two-photon reaction can provide a completely independent constraint on κ and λ which is of almost the same power at that from $e^+e^- \to W^+W^-$. Among other information, this constraint would resolve the two-fold ambiguity in Fig. 16. Some additional information can be obtained by studying the single W production process $e^-\gamma \to W^-\nu$, either in $e^-\gamma$ or in e^+e^- mode.

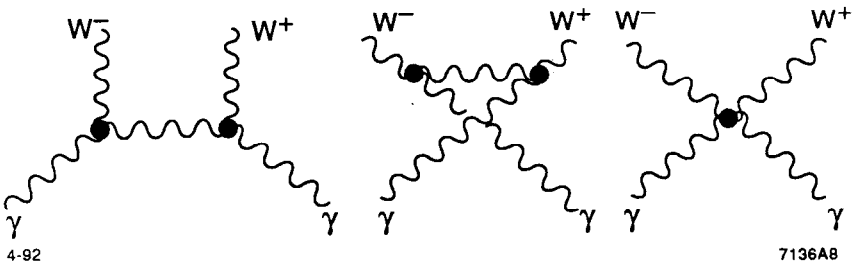

Figure 17. Leading-order diagrams contributing to $\gamma\gamma \to W^+W^-$.

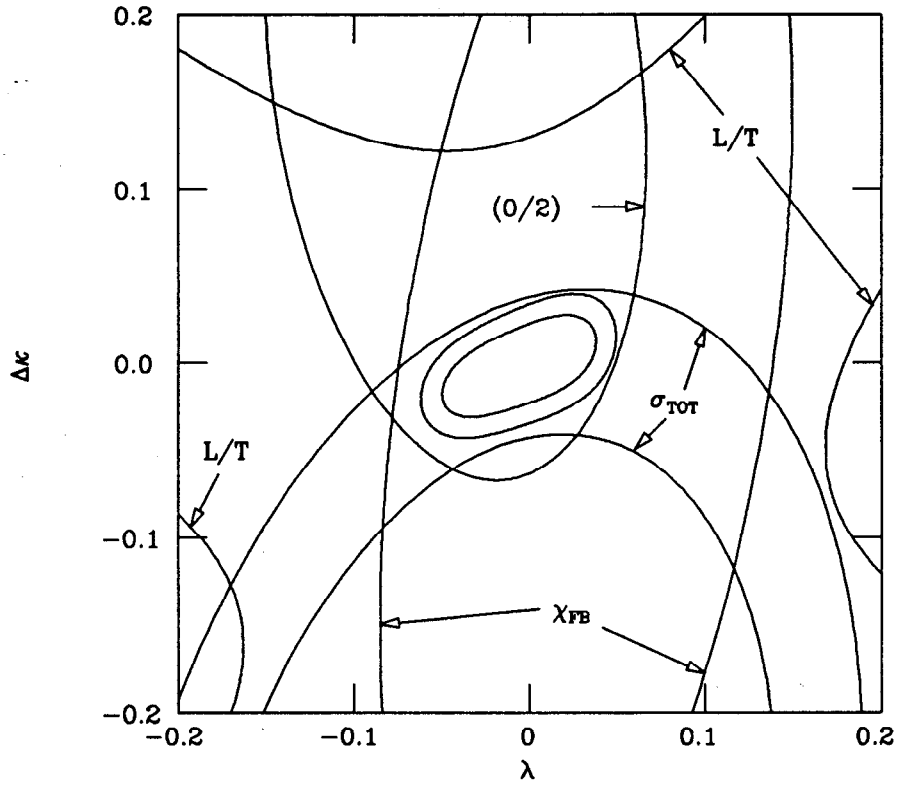

Figure 18. Expected bounds on the parameters κ, λ of the W anomalous couplings expected from the measurement of various features of the cross section for $\gamma\gamma \to W^+W^-$ at $\sqrt{s} = 500$ GeV, from Ref. 12.

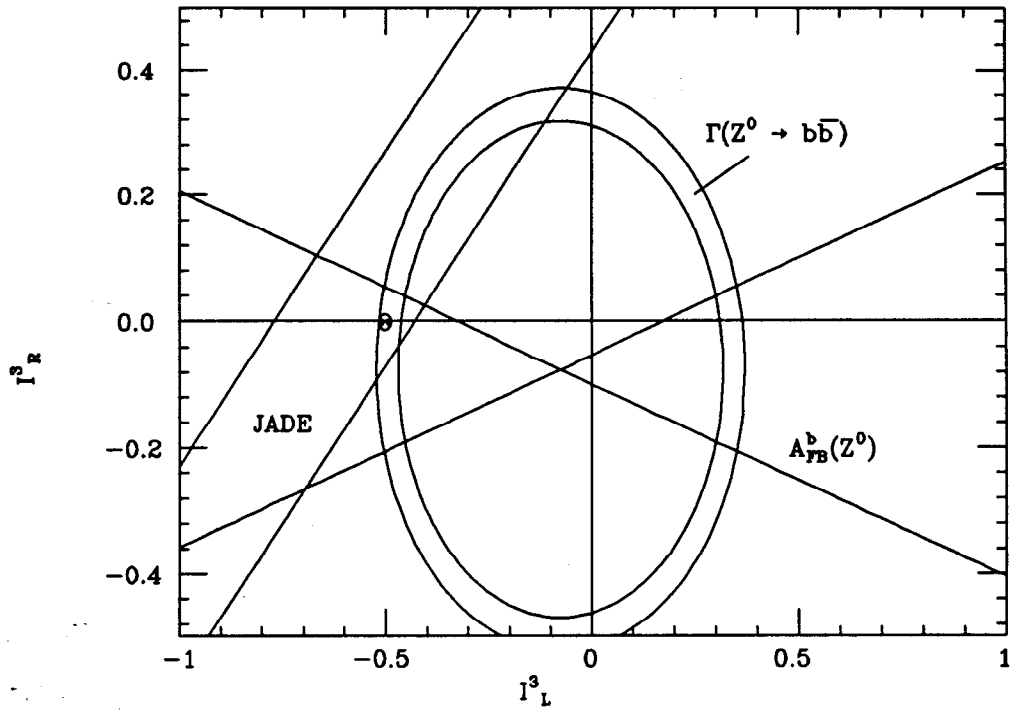

Figure 19. Determination of the weak isospin of the left- and right-handed components of the b quark. The three constraints overlap in a small region which contains the standard model result (marked with a circle).

5. The Top Quark

The third element of the standard model which can be studied at the NLC, and possibly the most interesting of all, is the top quark.

5.1 Issues for the Study of the Top Quark

Though the top quark has not yet been discovered, particle physicists generally consider it to be an established part of the standard model. In my opinion, this confidence in the existence of the top quark is justified. The reasoning is presented in Fig. 19. I assume the correctness of the $SU(2) \times U(1)$ model of the W and Z couplings to fermions; this model has now been amply tested in low-energy weak interactions and at LEP. According to this model, the couplings of the b quark to

the weak interactions are completely characterized by its $SU(2) \times U(1)$ quantum numbers. Conversely, we can use the the weak-interaction properties of the b quark to determine the charge assignments of its right- and left-handed components under the weak-interaction $SU(2)$. Even if we begin with arbitrary weak isospin assignments I_L^3, I_R^3, these values are strongly constrained by the LEP measurements of the Z^0 branching ratio to $b\bar{b}$ and the $b\bar{b}$ forward-backward asymmetry,[36] as shown in Fig. 19. These measurements leave a two-fold ambiguity which is resolved by a lower-energy measurements of the forward-backward asymmetry, which depends on the interference of γ and Z^0 contributions.[37] The data single out the assignment $(I_L^3, I_R^3) = (-\frac{1}{2}, 0)$, the conventional standard model expectation.[38]

In addition to the clear statement that the top quark exists, the precision electroweak experiments give some constraint on its mass. The effect of virtual top quark loops on observables gives a constraint which is most clearly written

$$(100 \text{ GeV})^2 < [m_t^2 + \mathcal{M}] < (180 \text{ GeV})^2, \tag{15}$$

where the quantity $\mathcal{M}$ is very small in the minimal standard model and is positive in most generalizations of the standard model.[39] The influence of the virtual top quark on $B\overline{B}$ mixing gives a weaker constraint which also puts the top quark in this general mass region. Thus, we already have some confidence that the threshold for $t\bar{t}$ production is below 400 GeV. In fact, these bounds imply a reasonable probability that the top quark will be discovered at the Fermilab collider in its coming run.

It is thus likely that the top quark will be discovered before the beginning of the physics program at the NLC, at a mass which puts it well within the energy reach of this machine. That opens an opportunity for NLC experiments, because the discovery of the top quark will open a number of new and interesting issues. Among these are:

1. The top quark mass: Hadron colliders will be able to measure the top quark mass to about 5 GeV.[40] But Blondel, Renard, and Verzegnassi[41] have argued that one must know the top quark mass to 1 GeV to take full advantage of the constraints that precision electroweak measurements put on the Higgs boson and other massive particles which might contribute to electroweak loops. Beyond this, it would be wonderful to make a precision measurement of the basic parameter m_t, to 300 MeV or better.
2. The top quark Yukawa coupling: In the minimal standard model, the top quark is not heavy enough to be strongly coupled to the Higgs sector, since the top quark-Higgs Yukawa coupling λ_t obeys the relation

$$\frac{\lambda_t^2}{4\pi} = \frac{1}{4\pi}\left(\frac{m_t}{v}\right)^2 = \frac{1}{34}, \tag{16}$$

using $m_t = 150$ GeV and v from (7). This is comparable to the value of the

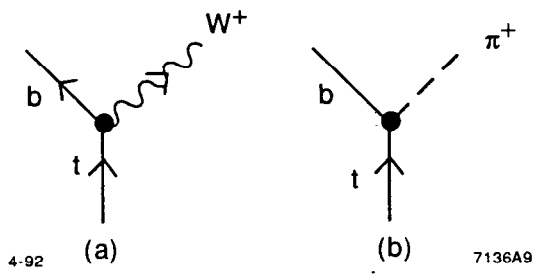

Figure 20. (a) The major top quark decay process $t \to W^+b$; (b) the process $t \to \pi^+b$, which determines the properties of top decay through Goldstone boson equivalence.

weak-interaction coupling $\alpha_w = g^2/(4\pi) = 1/30$. In models with more general Higgs sectors, this value could well be quite different, and it is interesting to speculate that it could become large enough to give the top quark strong Higgs interactions. Ideally, we should understand their relation experimentally, by measuring λ_t independently of m_t.

3. The top quark width: Γ_t can be smaller than the standard model prediction if V_{tb} is substantially less than 1, due to mixing of the top with new high-mass fermions, or it can be larger than the standard model value if the top quark has exotic decays.

4. The top quark form factors: Either through mixing with heavy species or though strong interactions, the top quark might acquire exotic form factors—for example, an anomalous magnetic moment larger than the 3% shift of $(g-2)$ expected from QCD—whose appearance would signal new physics.

I will now argue that the NLC allows a variety of top quark experiments which can address this set of questions.

5.2 General Properties of the Top Quark

To introduce these experiments, I will first discuss some general properties of the top quark. The distinguishing property of the top quark is, of course, its large mass. Since the top quark is heavier than the W, this large mass leads to an especially rapid decay, via $t \to W^+b$, shown in Fig. 20(a). If we can ignore the b quark mass, the rate of this decay is:[42]

$$\Gamma(t \to W^+b) = \left[\frac{g^2}{64\pi}\frac{m_t^3}{m_W^2}\right] \cdot \beta^3 \cdot \left(1 + 2\frac{m_W^2}{m_t^2}\right), \tag{17}$$

with $\beta = (1 - m_W^2/m_t^2)$. For $m_t = 150$ GeV, Γ_t is about 1 GeV.

A striking feature of (17) is its strong increase with the top quark mass: The expression is proportional to m_t^3. This feature is actually easy to understand by invoking Goldstone Boson Equivalence. The expression in brackets in (17) is the value of the decay width which would be obtained from the process shown in Fig. 20(b), the decay of the top quark to a b plus a massless Goldstone boson: In this calculation, two of the factors of m_t arise from λ_t^2, the square of the top quark Yukawa coupling.

The top quark is thus short-lived. In fact, it decays so rapidly that the top quark has no conventional meson spectroscopy: Not only are there no T meson tracks, there are no T mesons, or even toponium states near threshold.[43] However, as the convention mesons disappear, new principles of quark dynamics come into play. This point has been especially emphasized by Fadin and Khoze,[44] who have pointed out that the propagator of the unstable top quark is off-shell by an amount $(m_t\Gamma_t)$. Thus, this quantity, equal to (30 GeV)^2 for m_t = 150 GeV, acts as an infrared cutoff which justifies the use of QCD perturbation theory. Thus, nonperturbative physics is unimportant from the start of a top quark's life until its end, giving us an unprecedented opportunity to understand the couplings of this quark by comparing experiments to high-precision theoretical calculations.

5.3 The $t\bar{t}$ Threshold

I will first discuss the properties of $t\bar{t}$ production just at the quark-antiquark threshold, in the region normally occupied by the quarkonium resonances. Because of the rapid decay of the top quark, there are no narrow $t\bar{t}$ resonances; the individual t and $\bar{t}$ lifetimes set an upper limit to the lifetime of the bound state. However, the $t\bar{t}$ cross section in this region is still sensitive to the quark-antiquark binding potential. In fact, as Fadin and Khoze first pointed out,[44] the situation is the best one for extracting a detailed understanding of this interaction: The top or antitop decays at a separation $\Delta r = (m_t\Gamma_t)^{-1/2}$ where the QCD binding is strong but is determined entirely by perturbation theory.

The most important observable is the energy-dependence of the total cross section for $t\bar{t}$ production, over an energy interval of about 10 GeV near the threshold. In Fig. 21, I have plotted the behavior of the cross section expected from QCD for the top mass values 120 GeV, 150 GeV, and 180 GeV.[45] The cross sections are given in units of R and are plotted against $E = \sqrt{s} - 2m_t$. They are corrected for initial-state radiation, but not for machine-dependent effects. Over this mass range, the 1S $t\bar{t}$ resonance becomes smeared by the top quark width and spreads out to merge with the $t\bar{t}$ continuum. The very fact that the threshold has the shape of a sharp rise from zero to almost a unit of R implies that, by locating this rise, we can obtain a very

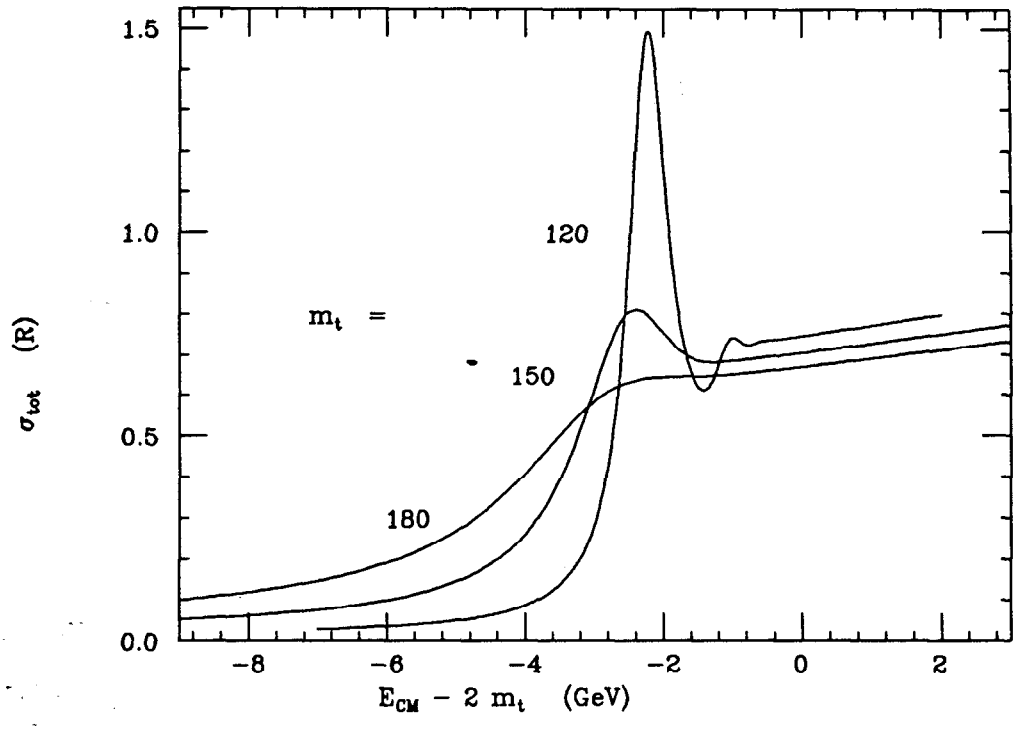

Figure 21. Comparison of the forms of the $t\bar{t}$ production threshold for $m_t = 120$, 150, 180 GeV. Note that the total cross section for $t\bar{t}$ production is plotted against the center-of-mass energy displacement ($E_{CM} - 2m_t$).

accurate determination of the top quark mass. In addition, the detailed shape of the cross section depends on properties of the top quark and its interactions through QCD and possible heavier exchanges. In Fig. 22, I show the variation of the prediction for $m_t = 150$ GeV with α_s; the three curves correspond to $\alpha_{s,\overline{MS}}(m_Z^2) = 0.11$, 0.12, 0.13; the separation is the current experimental error. Equally striking effects are produced by more exotic variations of the top quark physics: In Fig. 23, we can see effect of varying the top quark width. Adding the Higgs boson of the minimal standard model, with $m_H = 100$ GeV, has the effect shown in Fig. 24; this figure also shows the effect of nonstandard modification of the magnitude of the top-Higgs coupling λ_t. (The Higgs mass should not be taken as a parameter, since any Higgs boson mass in the relevant range will already have been measured in the NLC experiments discussed in Section 3.)

It should be noted that the threshold structure varies significantly when the energy is changed by a few GeV—that is, by less than a percent of the total center-

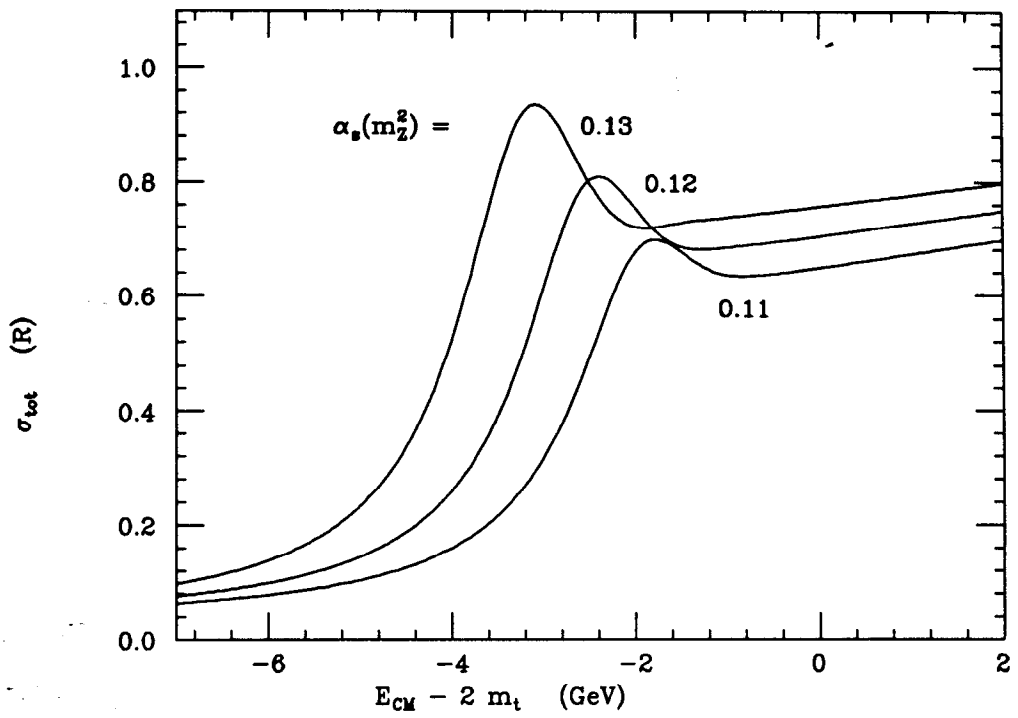

Figure 22. Comparison of the forms of the cross section for $t\bar{t}$ production near threshold, for $m_t = 150$ GeV, for $\alpha_s = 0.11, 0.12, 0.13$.

of-mass energy. To allow experiments to fully observe this threshold structure, accelerator designers should strive to produce a machine which, at least at its lowest energies, has an intrinsic energy spread at the collision point of less than 0.1 %. This is straightforward,[46] but it has not been incorporated into most current designs. Energy smearing by beamstrahlung is expected to be less important. Further details of the experimental study of the $t\bar{t}$ threshold are presented in Fujii's article in this volume.[47]

5.4 Top Quark Pair Production

A different and equally interesting set of observations is available well above threshold, in the region of open $t\bar{t}$ production. The optimal place to observe $t\bar{t}$ events is at an energy where the top quarks are fast but not completely relativistic, roughly 100 GeV above threshold. Even at these energies, the full structure of a $t\bar{t}$ event is

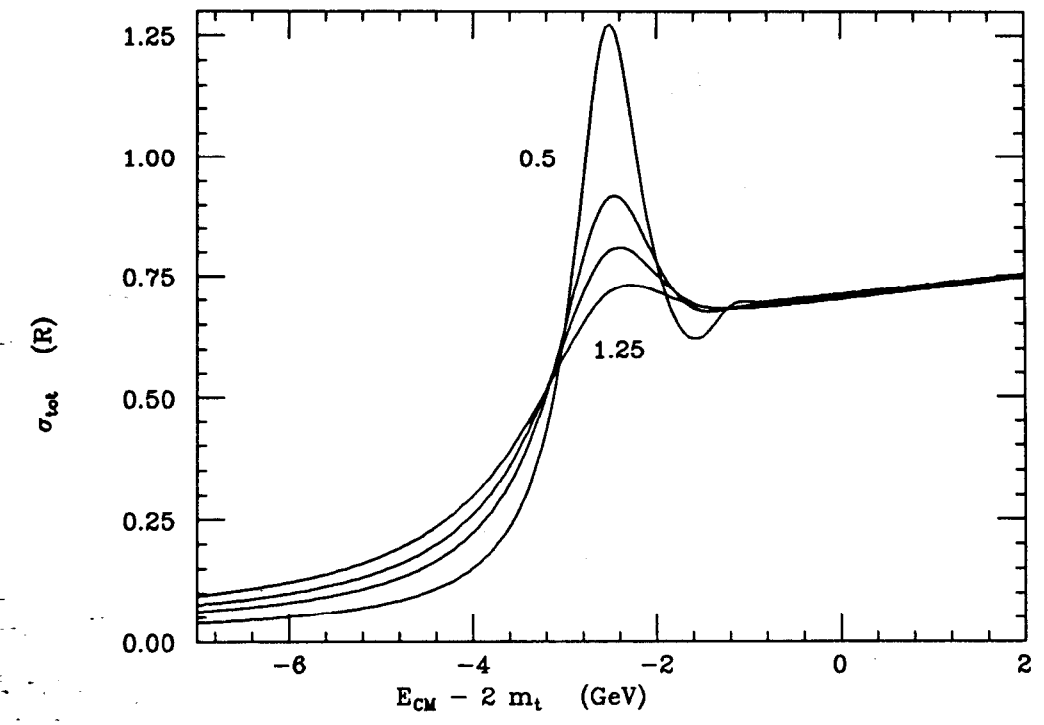

Figure 23. Comparison of the forms of the cross section for $t\bar{t}$ production near threshold, for $m_t = 150$ GeV and $\alpha_s = 0.12$, as the width of the top quark is taken to be 0.5, 0.75, 1.0, and 1.25 times its standard model value.

rather complicated: Each top quark decays to Wb, which results eventually in either three jets or a jet, a lepton, and a neutrino, on each side of the event. However, simulations of this process show that, in the uncluttered environment of e^+e^- collisions, these events can be easily separated from backgrounds and the full structure of the final state can be reconstructed.[47] An essential element of this reconstruction is the fact that the six-jet system obeys a large number of mass constraints: Two pairs of jets each sum to the mass of the W, and for each of these the addition of a third jet produces a system with the mass of the t. Further, if we ignore the relatively small effects of initial state radiation, beamstrahlung, and gluon radiation, each of these reconstructed top quarks has just the energy of the electron beam.

The full reconstruction of $t\bar{t}$ events produces a wealth of information: The process depends on a production angle θ and polar and azimuthal decay angles for the t, $\bar{t}$, W^+ and W^-. In the process $e^+e^- \to W^+W^-$, we found that some of the most interesting information is contained in the correlations among these parameters; these measure

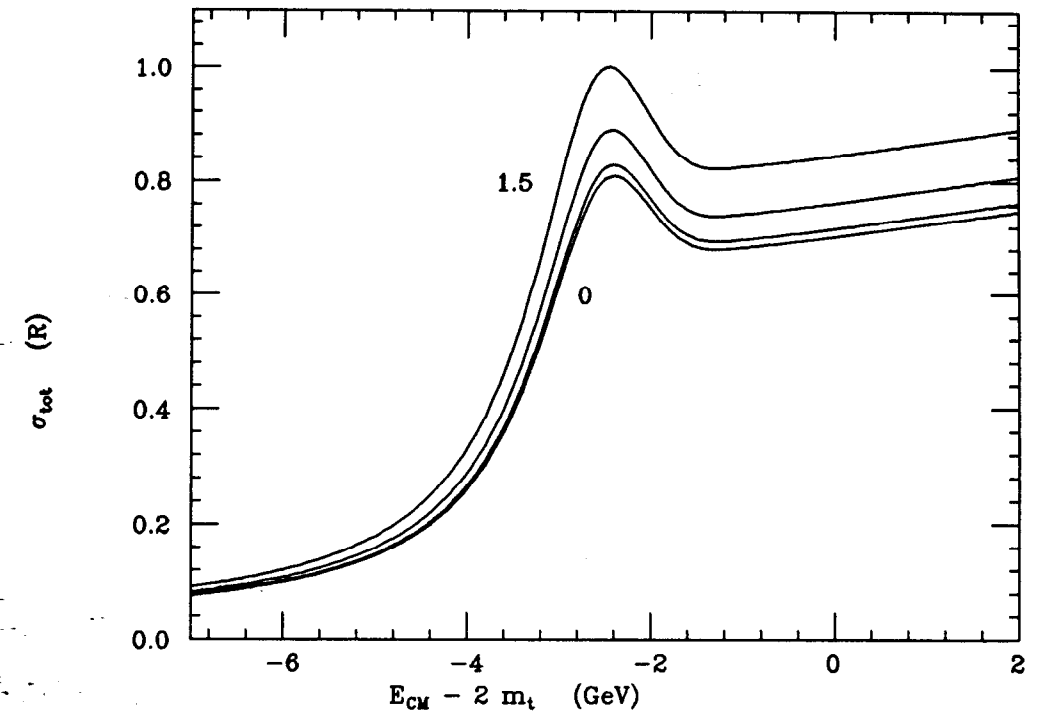

Figure 24. Comparison of the forms of the cross section for $t\bar{t}$ production near threshold, for $m_t = 150$ GeV, $\alpha_s = 0.12$, and a Higgs boson mass of 100 GeV, as the coupling of the Higgs boson is taken to be 0, 0.5, 1.0, and 1.5 times its standard model value.

quantities such as the fraction of longitudinally polarized W's produced at backwards angles which are highly sensitive to perturbations of the standard model. In the top system, these correlations are more complex. As in W pair production, howver, they are best untangled and understood by analyzing the process of $t\bar{t}$ production and decay in terms of intermediate-state helicities.

For lighter quarks, helicity is not a useful tool because the quark spin direction is randomized during hadronization. For example, a polarized b created in a high-energy collision evolves into a coherent mixture of B and B^* mesons. At times of order $(m_{B^*} - m_B)^{-1} \approx (50\ \text{MeV})^{-1}$, these components become incoherent, and at this point the original spin orientation is lost. Even later, the B^*'s decay to B's, completing the randomization of the b quark spin. We have already noted that, for heavy top quarks, there is no hadronization process; the evolution from the initial t quark to the decay products W^+b is governed by QCD perturbation theory. The point applies even more strongly to the spin exchange time, since its inverse, the spin

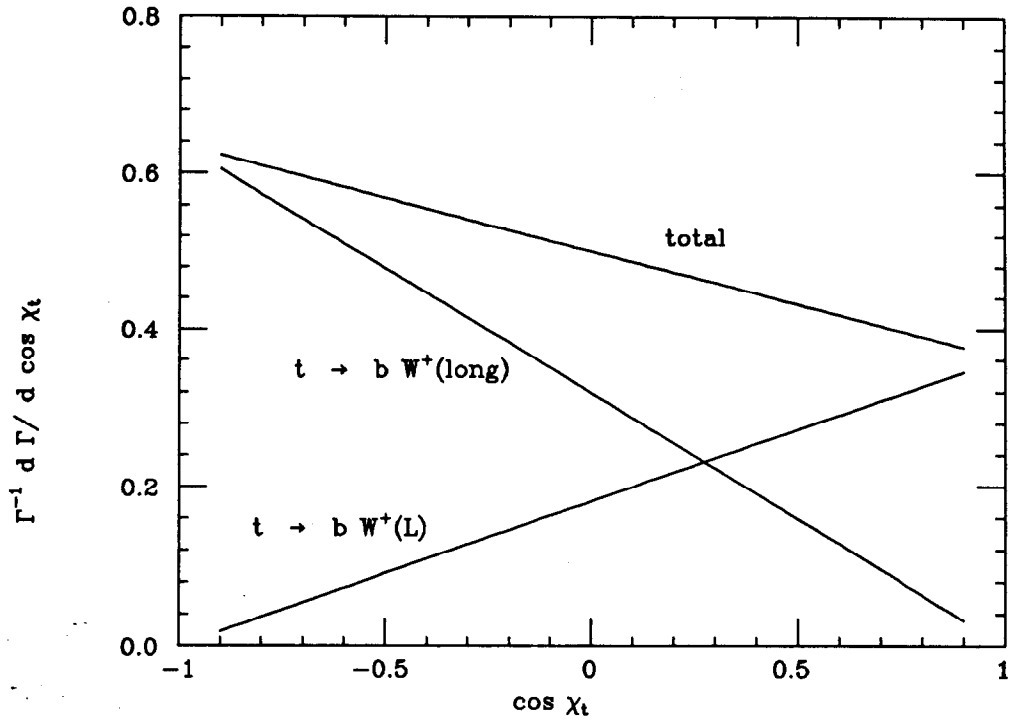

Figure 25. Distribution of top quark decay events in the decay angle χ, computed for left-handed polarized top quarks. The distributions are shown both for the total decay rate and for the individual decay channels to longitudinally polarized W bosons.

exchange energy, varies as m_t^{-1} as the top becomes heavy. For a 150 GeV top quark, scaling from the b, we would expect a spin exchange energy of (50 MeV) $\cdot$ (m_b/m_t)); this gives a spin exchange rate of (2 MeV), orders of magnitude less than the t decay rate. Thus, for top, the quark spin is a useful parameter. We will see in a moment that both the production and decay distributions of top have an essential spin dependence which can be measured experimentally.

To explain the properties of open top events, I will first present the predictions of the tree level standard model for the various components of this process, expressed in a basis of states of definite helicity. Once we have this foundation, we can combine these helicity amplitudes to see the full structure of the event.[48,49]

We have already discussed the process of W decay, and the dependence of the distribution in the W^+ decay angle χ on the W^+ helicity. For the purposes of this study, it is most convenient to measure the W^+ direction and thus the W^+ helicity in the frame of the t quark. Then the same helicity basis can be used to describe

the t decay. Define the decay angle χ_t as the angle between the t direction and the W direction, measured after boosting the top quark to rest. At tree level, and ignoring the mass of the b, the standard model makes very simple predictions for the dependence of the t decay amplitudes on χ_t. The b is always left-handed, and so by angular momentum conservation it can recoil only against a left-handed or longitudinal W^+. For a left-handed top quark, the decay amplitudes are

$$\begin{aligned} \mathcal{M}(t_L \to bW_L^+) &= -ig(m_t^2 - m_W^2)^{1/2} \cos\frac{\chi_t}{2} \\ \mathcal{M}(t_L \to bW_{long}^+) &= -ig(m_t^2 - m_W^2)^{1/2} \left[\frac{m_t}{\sqrt{2}m_W}\right] \sin\frac{\chi_t}{2}, \end{aligned} \tag{18}$$

where χ_t is the t decay angle. The two amplitudes lead to angular distributions proportional to $(1 + cos\chi_t)$ and $(1 - \cos\chi_t)$, respectively. The quantity in brackets in the second line of (18) is an enhancement which raises the strength of the tbW coupling from g to λ_t for the longitudinal W; this is just what we should expect from Fig. 20 and the Goldstone Boson Equivalence Theorem. For $m_t = 150$ GeV, 65% of t decays have a longitudinal W in the final state. This produces the χ_t distribution shown in Fig. 25; the decay distribution of the top is quite an effective polarization analyzer.

The production process $e^+e^- \to t\bar{t}$ depends on θ and on the electron and top quark polarizations. As usual in e^+e^- annihilation to fermions, the helicity conserving reactions leading to $t_L\bar{t}_R$ and $t_R\bar{t}_L$ have differential cross sections proportional to:

	$t_L\bar{t}_R$	$t_R\bar{t}_L$
$e_L^-e_R^+$	$(1+\cos\theta)^2$	$(1-\cos\theta^2)^2$
$e_L^+e_R^-$	$(1-\cos\theta)^2$	$(1+\cos\theta^2)^2$

(19)

However, the sizes of these cross sections are very different, because the couplings of the Z^0 depend strongly on the helicities and because, in this energy region well above m_Z, photon-Z^0 interference is very important. For $s >> m_Z^2$, each helicity cross section is multiplied by a factor

$$|f|^2 = \left|-\frac{2}{3} + \frac{(I_e^3 + \sin^2\theta_w)(I_l^3 - (2/3)\sin^2\theta_w)}{\sin^2\theta_w \cos^2\theta_w}\right|^2. \tag{20}$$

For the four channels in (19), the four factors $|f|^2$ are

	$t_L\bar{t}_R$	$t_R\bar{t}_L$
$e_L^-e_R^+$	1.4	0.2
$e_L^+e_R^-$	0.05	0.75

(21)

This means that the annihilation of $e_L^-e^+$ to $t\bar{t}$ has a very large forward-backward asymmetry. Further, this asymmetry is correlated with top polarization; essentially

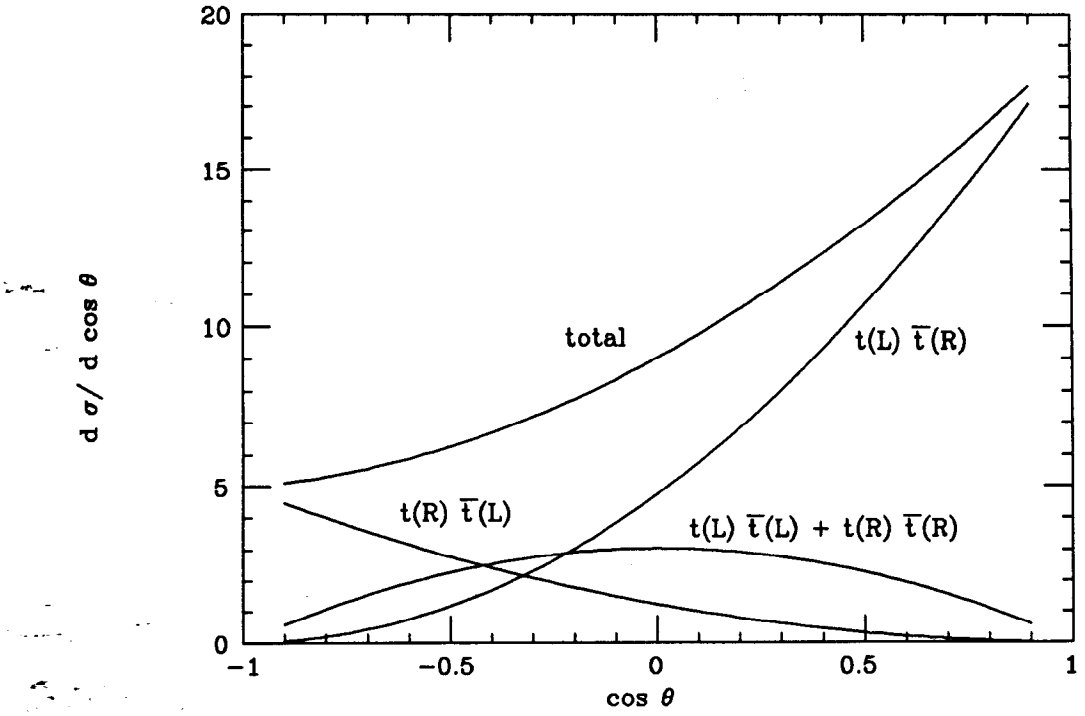

Figure 26. Distribution of $e^+e^- \to t\bar{t}$ events in the production angle θ, computed for left-handed polarized electrons. The distributions are shown both for the total rate and for the contributions of the individual t and $\bar{t}$ polarization states.

all t quarks produced at $\cos\theta > 0.5$ are left-handed. The $t\bar{t}$ angular distribution for $e^-_L e^+$ annihilation, and its decomposition into helicity states, is shown in Fig. 26. For $e^-_R e^+$ annihilation, the cross sections have roughly the same shape, after interchange of t_L, $\bar{t}_R$ with t_R, $\bar{t}_L$, but they are about a factor of two smaller. Thus, the large forward-backward and polarization asymmetries should persist even for unpolarized beams.

The many distinctive features of the standard model process of $t\bar{t}$ production and decay make it possible to design experimental tests for individual top quark form factors which might appear from physics beyond the standard model. To illustrate this point, I will discuss the measurement of the decay form factors of an individual top quark.[50] Let us assume that we have a sample of left-handed polarized top quarks; I have already explained how this can be obtained using a polarized e^- beam and a cut which selects forward production angles. Each of the processes of (18) has a characteristic dependence on $\cos\chi_t$, which follows from this equation, and on $\cos\chi$,

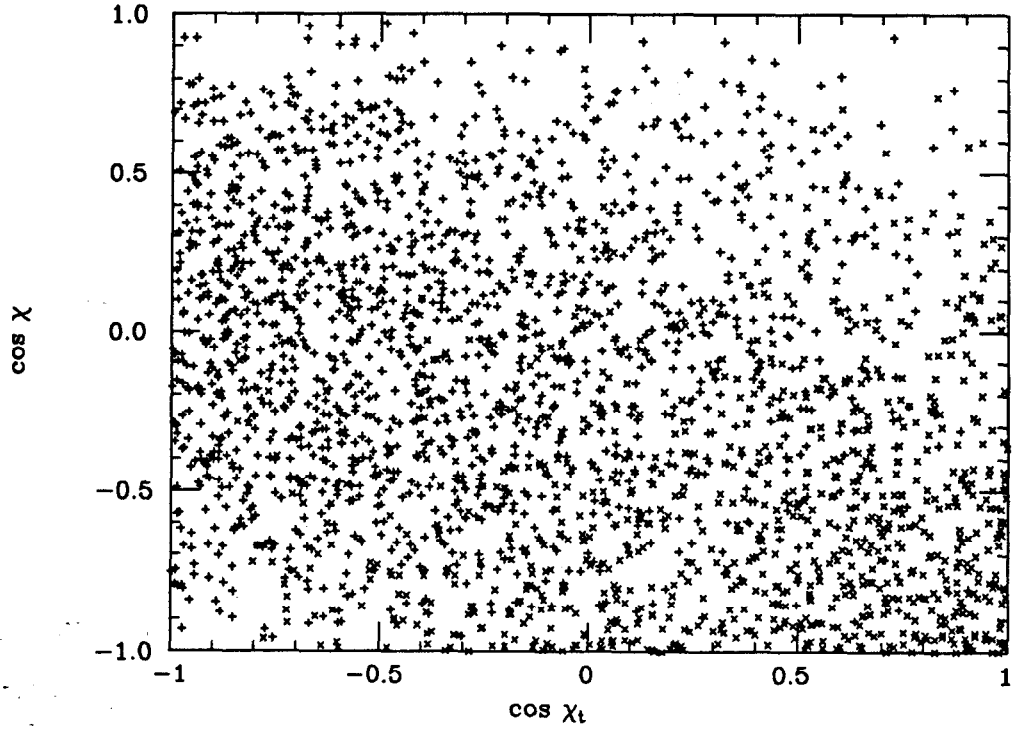

Figure 27. Scatter plot of the decays of a left-handed top quark in the t decay angle χ_t and the W^+ decay angle χ. Events with longitudinal W bosons are marked +; events with left-handed W bosons are marked ×. This distribution is an appropriate starting point for the analysis of anomalous couplings in top decay.

according to the W^+ polarization. A scatter plot of these events on the plane of $\cos\chi_t$ vs. $\cos\chi$ is shown in Fig. 27. Anomalous form factors at the t decay vertex show up as changes in the event distribution in this plane. For example, a magnetic-moment coupling at the decay vertex enhances the production of W_L^+ relative to W_{long}^+, enhancing the density of events in the bottom right-hand corner of the plot. Another possible modification is the presence of a decay of the top quark to a right-handed b ($t \to W^+ b_R$) as the result of the mixing of the t with a heavy 'mirror' fermion. The events from this process would appear in the upper right-hand corner of the plot and so would be easy to identify or rule out. The principal background to this effect is the higher-order QCD process $t \to W_R^+ bg$; however, its rate is only 10^{-3} of the tree-level decay rate.

Form factors at the production vertex can be identified by similar analyses which make use of the $\cos\theta$ distributions and the correlations between the t and $\bar{t}$ decays.

For example, an anomalous magnetic moment form factor selectively enhances the helicity flip processes $e^+e^- \to t_L\bar{t}_L,\ t_R\bar{t}_R$. This reaction depends on energy and production angle according to

$$\frac{d\sigma}{d\cos\theta} \propto \left|\frac{m_t}{E_t}(F_{1L}+F_{1R}) + \frac{E_t}{m_t}(2F_2)\right|^2 \cdot \sin^2\theta, \tag{22}$$

where $F_{1L,R}$ are the (handed) charge form factors and F_2 is the magnetic form factor, and leads to its own characteristic pattern in the space of production and decay angles.

In principle, it should be possible to separately measure all of the various production and decay form factors of the top quark, at the level of a few percent. This study could provide the best determination available of the fundamental pointlike couplings of a quark. Alternatively, it might well show anomalous vertices of the top quark which signal its coupling to a strongly interacting sector associated with mass generation.

6. Physics Beyond the Standard Model

So far, I have discussed only those aspects of the NLC physics program which are contained within the minimal standard model. The study of W^+W^- and $t\bar{t}$ production and the definitive search for Higgs bosons below 200 GeV provide in themselves a rich experimental program for a 400–500 GeV e^+e^- collider, whatever the scale of truly new phenomena turns out to be. However, it would be silly to ignore the fact that the NLC has powerful capabilities for studying any new phenomena that appear in its mass range.

This subject of searching for new particles at e^+e^- colliders is, paradoxically, more familiar than the subjects of the previous few sections, since these searches have been a major part of the experimental program at PEP, PETRA, TRISTAN, and LEP. Particularly useful summaries of these lower-energy studies have been given by Komamiya[51] and Davier.[21]

In this section, I will concentrate on two specific schemes for physics beyond the standard model: supersymmetry and the strongly interacting Higgs boson. I consider these particularly important models, because they are the two main competitors for the explanation of the mechanism of $SU(2) \times U(1)$ symmetry breaking. In deference to the enormous literature on each of these subjects, I will only discuss aspects of these models which have particular relevance for linear collider experiments.

Before discussing specific items, though, I should note one major difference between particle searches at the NLC and searches at previous e^+e^- colliders. The basic mystery which leads to an expectation of new physics beyond the standard model

is the nature of the symmetry-breaking sector, the Higgs sector. The mass scale of this sector is presumable related to the one dimensionful quantity in the sector that we have measured, the parameter (7): $v = 250$ GeV. Up to now, particle searches at electron (or, for that matter, proton) colliders have excluded masses only up to a small fraction of this energy. The SSC and LHC will widen this search in hadronic phenomena. But among electron colliders, the NLC will be the first to enter the generic region of parameter space in which there is a substantial probability of a encountering the next scale of physics.

6.1 Supersymmetric Particles at the NLC

In this section, I will discuss a few of the particles of the supersymmetric extension of the standard model which might be found at the NLC. These include specifically supersymmetric states but also the interesting Higgs boson sector of the model. All specific predictions will refer to the minimal supersymmetric standard model.[52,53]

Supersymmetry requires the addition of a second Higgs doublet to the $SU(2) \times U(1)$ model, and this small modification brings in a number of new physical states: In addition to the single Higgs scalar h^0 of the minimal standard model, we now have a second neutral scalar H^0, a pseudoscalar A^0, and a pair of charged scalars $h^\pm$. Such new states appear whenever there are extra Higgs doublets, but in the general case their properties are quite model-dependent. Minimal supersymmetry makes definite predictions for these particles, which might be regarded either as interesting predictions in their own right or as properties of an interesting specific example from the general class of models with extended Higgs sectors.[20,54]

In minimal supersymmetry, the lighter scalar h^0 is usually more strongly coupled to Z^0Z^0; its production cross section in $e^+e^- \to h^0Z^0$ is almost as large as that of the Higgs boson in the minimal standard model discussed in Section 2.2. The mass of the h^0 has an upper limit which is sensitive to radiative corrections from a heavy top quark but which is of order 120 GeV for $m_t = 150$ GeV. This may be too heavy to be accessible at LEP II, but, for any reasonable value of m_t, lies within the range of the NLC. The heavier scalar H^0 has no definite upper limit to its mass, and the heavier it is, the more it decouples from Z^0Z^0. However, in this limit the process $e^+e^- \to A^0H^0$ in unsuppressed, except by the H^0 and A^0 masses (with $m_{A^0} < m_{H^0}$). When the masses of H^0 and h^0 become almost equal, the H^0 may predominate in the associated production with Z^0, but then the h^0 is produced equally strongly with A^0. Thus, if the H^0 is in the NLC mass range, all three states h^0, H^0, and A^0 are produced at reasonable rates. In any event, the h^0 can always be found. A detailed analysis of the search for these states is given in the article of Grivaz.[55]

Now I will turn to specifically supersymmetric states. Here I would like to make

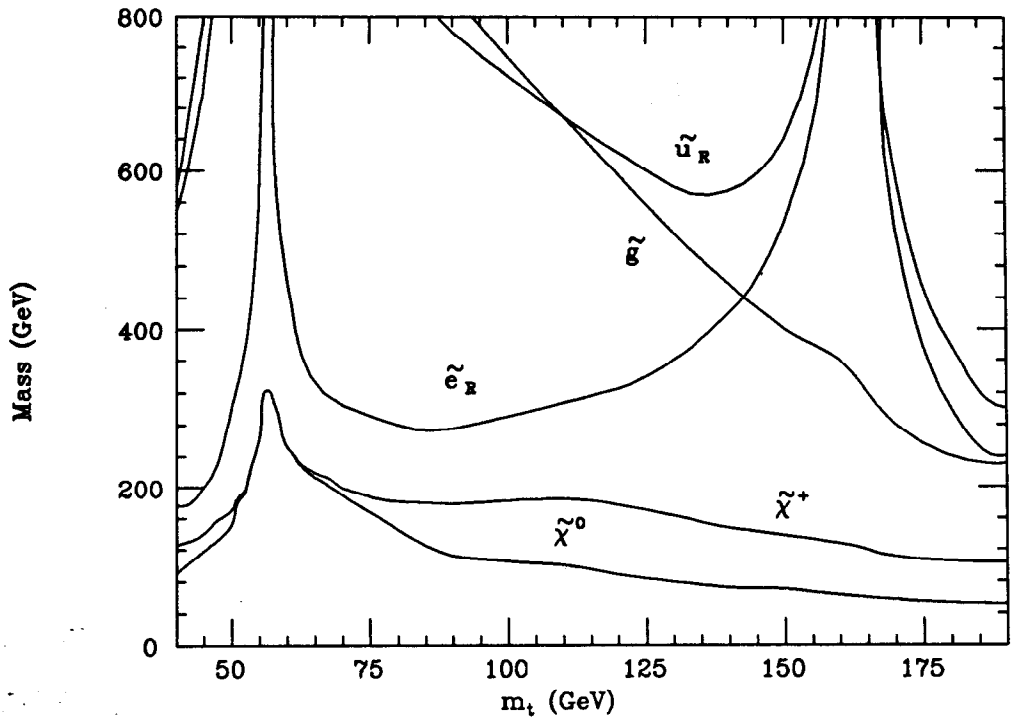

Figure 28. Limits on the masses of various species in the minimal supersymmetric standard model, according to the naturalness criterion of Barbieri, from Ref. 56.

three comments. First, though it is worth searching experimentally for all supersymmetric states, in most models the lightest states are the charginos χ^+ and neutralinos χ^0, the supersymmetric partners of W, Z, γ, and the Higgs bosons. Within the context of minimal supersymmetry and its embedding in grand unified models, Barbieri has proposed a naturalness condition that no parameter of the model should need to be fine-tuned by more than a factor of 10 to maintain the the Higgs vacuum expectation value v at its measured value well below 1 TeV.[56]The results of applying Barbieri's condition are shown in Fig. 28. The masses of the supersymmetric partners of quarks and leptons are constrained to lie below 1 TeV, but they can easily be in the range of 400–800 GeV. On the other hand, the masses of the χ^+ and χ^0 are strongly constrained to lie below 200 GeV. These are precisely the states which are difficult to find in hadron colliders but which are readily produced with distinctive signatures at e^+e^- colliders. If Nature is indeed supersymmetric, the NLC will carry out interesting experiments on charginos and neutralinos at the same time that the SSC explores the properties of squarks and gluinos.

The second point concerns the signatures of supersymmetric particles. In the search experiments which have been carried out to date, the desired signature of supersymmetric states is missing transverse momentum carried off by the lightest neutral superparticle. However, superparticles in the NLC mass range can decay by emitting W and Z bosons or Higgs bosons

$$\chi^+ \to W^+\chi^0 , \qquad \chi^{0\prime} \to h^0\chi^0$$

and the reconstruction of these states can form an important part of the experimental analysis. It is possible that W reconstruction may be more important than calorimetry for discovering supersymmetry at the NLC.

Third, once supersymmetry is discovered, this will be only the beginning of a long and fascinating story. The spectrum of supersymmetric particles is complex and its details are sensitive to the pattern of supersymmetry breaking. The NLC and higher energy e^+e^- colliders have an important role to play in the program of determining the fine details of the superspectrum, since they allow many incisive experimental probes of the superparticles and their decays. For example, the process of e^+e^- annihilation to squarks and sleptons has a large polarization asymmetry, of opposite sign for the superpartners of left- and right-handed fermions. Thus, the mass and branching fraction differences of $\tilde{e}_L^-$ and $\tilde{e}_R^-$, for example, can be studied in a controlled way.

In the minimal scheme of supersymmetry, the supersymmetry breaking terms, like the Higgs Yukawa couplings, come down from the scale of grand unification. They provide a new window through which we can glimpse physical processes at the deepest length scales. I would like to put on record my belief that, if a superstring model of Nature is correct, this model will be confirmed by its successful prediction of these soft supersymmetry breaking terms. In any case, the discovery of supersymmetry will open a new era of elementary particle physics, and it will be one in which e^+e^- linear colliders play an essential role.

6.2 The Strongly Interacting Higgs Sector

An alternative scheme for $SU(2) \times U(1)$ symmetry breaking involves the presence of a Higgs sector with strong interactions. This possibility appears in the minimal standard model for very large values of the Higgs boson mass, and also in technicolor or other models in which the Higgs boson is composite. The experimental manifestations of Higgs boson strong interactions occur mainly in the energy region above 1 TeV and so are inaccessible to a 500 GeV NLC. The discovery of these strong interactions is a major goal of the SSC, and much effort has been spent in analyzing

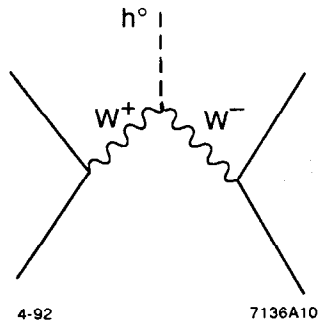

Figure 29. Higgs boson production by W^+W^- fusion.

the capabilities of the SSC for uncovering this physics, particularly through the W fusion reaction (Fig. 8(c) or Fig. 29). Unfortunately, the signals of Higgs strong interactions at hadron colliders are model-dependent and, for some models, may be difficult to extract.[57] Thus, it is worth considering what additional information e^+e^- colliders—not the NLC, but the TeV-energy machines of the future—will bring to this study.

The background for this discussion comes again from the Goldstone Boson Equivalence Theorem. In a theory in which the Higgs bosons have strong interactions, the strongly interacting states will include the massless Goldstone bosons associated with $SU(2) \times U(1)$ breaking. When this Higgs sector is coupled to the $SU(2) \times U(1)$ gauge bosons, these Goldstone bosons are absorbed into the longitudinal polarization states of W and Z bosons, which inherit their interactions. Among the backgrounds to the study of these strong interactions are the transversely polarized W and Z bosons, whose interactions remain those of conventional perturbation theory.

In this context, the W fusion process is interesting because it can proceed through a strong interaction amplitude. The contribution from longitudinally polarized W bosons measures the Goldstone boson scattering cross section

$$\frac{d\sigma}{d\cos\theta}(\pi^+\pi^- \to \pi^+\pi^-) \tag{23}$$

I have denoted the Goldstone bosons by $\pi^\pm$ to emphasize the analogy to the familiar strong interactions. This analogy is strong and very useful: Like the usual strong interactions, the Higgs sector must have a broken $SU(2)$ symmetry group and an additional unbroken $SU(2)$, the 'custodial symmetry' which assures that Veltman's ρ parameter is naturally close to 1.[58] The three Goldstone bosons form a iso-triplet under this unbroken global symmetry, just as the pions do under isospin. Thus, assuming always that the weak interactions are indeed described by an $SU(2) \times U(1)$ gauge theory, all relations following from the symmetries of the problem are identical between pion physics and the physics of strongly-interacting Higgs Goldstone bosons.

As I noted in Section 3.1, the W fusion reaction can also be studied in high energy e^+e^- reactions. However, detailed studies of this reaction show that there are formidable experimental problems.[8,59–61] Above 1 TeV in the WW center of mass, the rate of the W fusion process is quite low, requiring an the e^+e^- energy almost double the WW energy to be studied. This makes the task more difficult not only in the accelerator design but also in the data analysis: While reactions at the full e^+e^- energy are relatively free of background, reactions at half this energy or below receive large backgrounds from two-photon and photon-electron processes. Both of these reactions easily produce pairs of weak bosons, and one must use more detailed kinematic and polarization information to distinguish these from WW scattering.

However, there is another way that e^+e^- colliders can give new information about Higgs strong interactions, information which is, in fact, complementary to that coming from the proton colliders. To explain this point, I will first discuss the set of parameters which characterize a strongly interacting Higgs sector and then explain how these parameters can be measured.

The goal of studying WW scattering is to determine the $\pi\pi$ scattering amplitudes of the Higgs sector, in as many channels as possible. As in the familiar strong interactions, pion scattering channels are labeled by spin J and isospin (or custodial $SU(2)$) I. A simple but convenient representation of the $\pi\pi$ phase shifts is given by the effective range formula:

$$\cot \delta_{IJ} = \frac{A_{IJ}}{s}\left(1 - \frac{s}{M_{IJ}^2}\right). \tag{24}$$

For each partial wave, this formula has two parameters, A_{IJ} and M_{IJ}^{-2}. The values of A_{IJ} follow from current algebra and so are identical in the familiar and new strong interactions:

$$A_{00} = 16\pi F^2 \; ; \qquad A_{11} = 96\pi F^2 \; ; \tag{25}$$

where $F = f_\pi$ in hadron physics and $F = v$ in Higgs physics. The parameter M_{IJ}^{-2} can be either positive or negative; the notation in meant to suggest that, if the partial wave is resonant, M_{IJ} is the resonance mass.

This parametrization provides a useful semiquantitative description of a variety of models for the strongly interacting Higgs sector.[62] The values of A_{IJ} are universal predictions of $SU(2) \times U(1)$. The values of M_{IJ}^{-2} distinguish specific models of the strongly interacting Higgs sector. In the familiar strong interactions, the channels with the strongest $\pi\pi$ scattering are $I = J = 0$ and $I = J = 1$, and it is likely that this is true in the most general models of pion physics. Then it is interesting to consider the predictions of any given model for M_{00}^{-2} and M_{11}^{-2} In Fig. 30, I show the predictions for these parameters from technicolor models, with a prominent techni-ρ

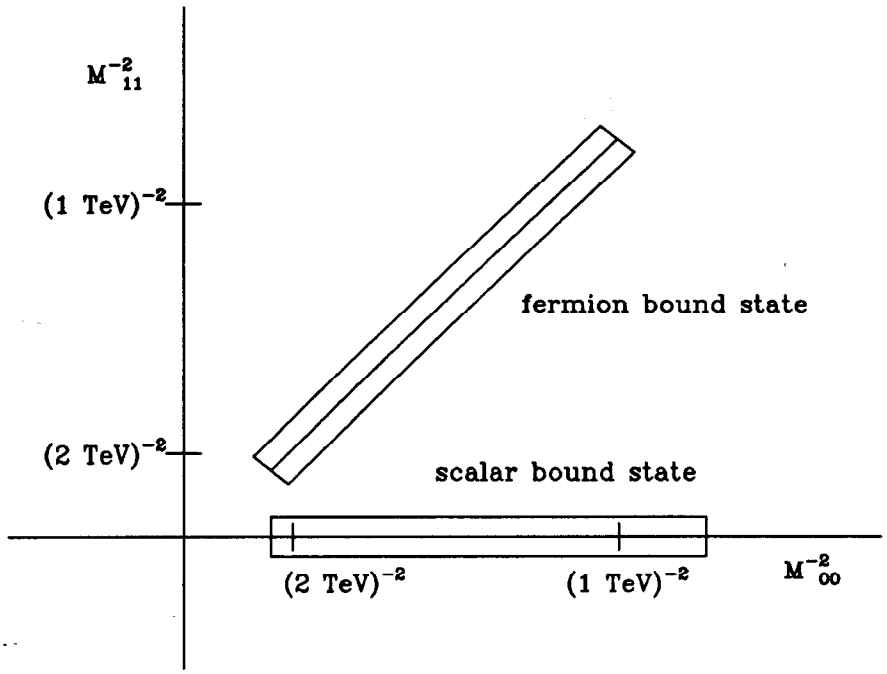

Figure 30. The parameter space of the models of the strongly interacting Higgs sector: M_{00}^{-2} vs. M_{11}^{-2}.

resonance, and from models in which the Higgs sector is built of strongly interacting scalars. To test these predictions, we must determine the true point in this plane experimentally.

I have already noted that this can be done in hadron colliders by measuring the strengths of WW and WZ scattering processes. But there is an alternative method, one which is well suited to the experimental advantages and constraints of e^+e^- colliders. We can measure the correction to electroweak production of vector boson pairs due to their final-state interactions. Even when this correction is small, they can be observed as well-normalized deviations from a precisely computed theoretical expectation. For transversely polarized vector bosons, the effect is quite small, but for longitudinally polarized bosons, the effect can be large and is directly associated with Goldstone boson strong interactions. In addition, different electroweak reactions project onto different $\pi\pi$ partial waves, sampling the functions (24) individually.

The largest effect arise in the reaction $e^+e^- \to W^+W^-$. When this process produces longitudinally polarized W pairs, these appear in the $I = J = 1$ partial wave and rescatter through the corresponding phase shift. The final state interaction can be described by an Omnés function[3,63]

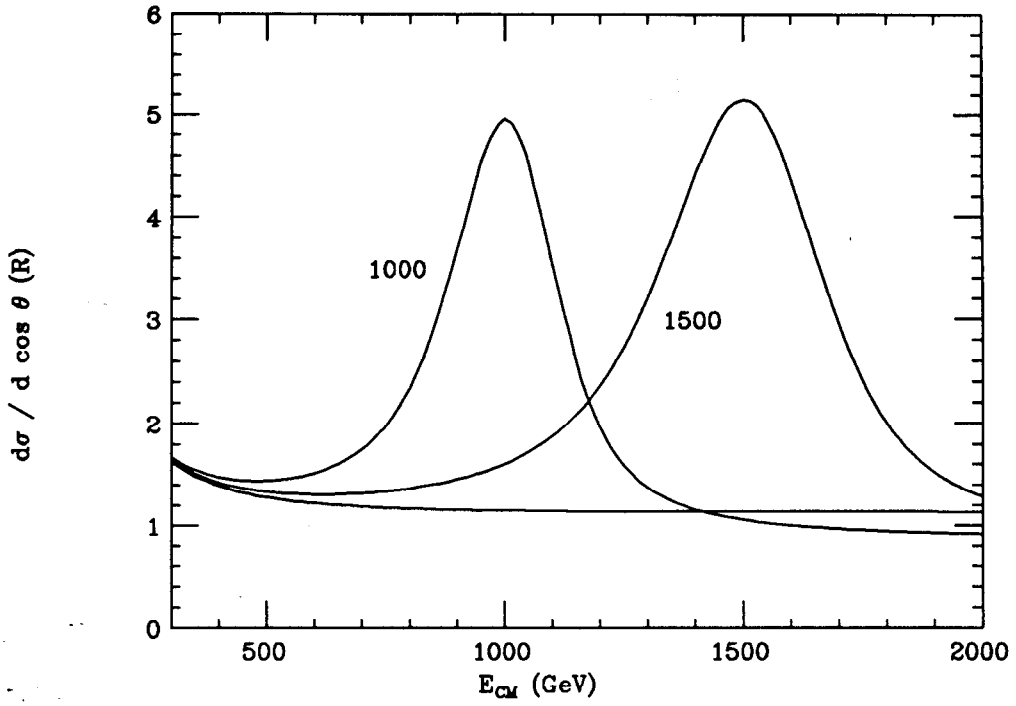

Figure 31. Effects of W^+W^- final state interaction on the differential cross section for $e^+e^- \to W^+W^-$ at $\cos\theta = 0.0$, using a phase shift δ_{11} with a resonance at masses of 1 TeV, 1.5 TeV, compared to the case of no rescattering.

$$\mathcal{M}(e^+e^- \to W_{long}{}^+W_{long}{}^-) = \mathcal{M}_0(e^+e^- \to W_{long}{}^+W_{long}{}^-) \cdot \exp\Big[\frac{s}{\pi}\int \frac{ds'}{s'(s'-s)}\delta_{11}(s')\Big]. \tag{26}$$

In this formula, $\mathcal{M}_0$ is the lowest order electroweak amplitude and the exponential gives a form-factor enhancement. For models with low-lying $I = J = 1$ ('techni-ρ') resonances, this enhancement can be a major effect, even if no attempt is made to separate transverse and longitudinal W's. This is shown in Fig. 31; in this figure, predictions for strongly resonant phase shifts are compared to the case of no rescattering, which is essentially the prediction of the standard model with a light Higgs boson. Resonances this prominent can also be seen easily at hadron colliders. The real power of e^+e^- annihilation is shown in Fig. 32, where we see that a precision study of the W pair production cross section can reveal resonant structure at several times the e^+e^- center-of-mass energy. Even the case $M_{11}^{-2} = 0$, which has

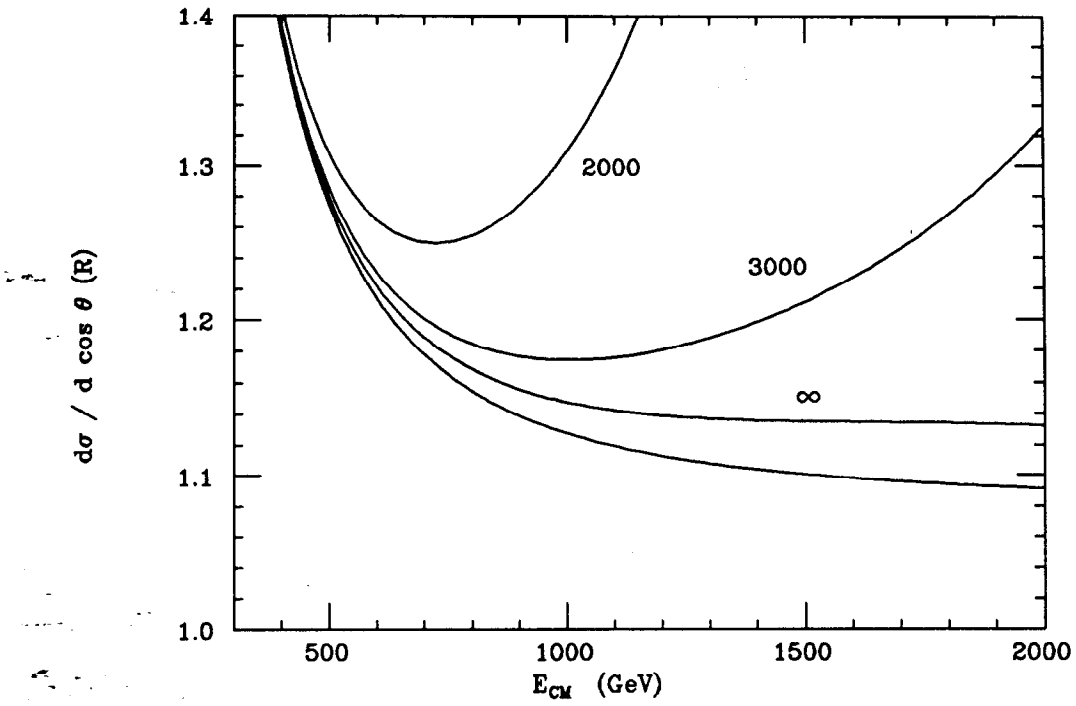

Figure 32. Effects of W^+W^- final state interaction on the differential cross section for $e^+e^- \to W^+W^-$ at $\cos\theta = 0.0$, using a phase shift δ_{11} with a resonance at masses of 2 TeV, 3 TeV, and ∞, compared to the case of no rescattering.

no significant consequences at hadron colliders, leads to an effect which differs from the prediction of weakly-coupled Higgs models by about 3% in the differential cross section and 5% in the corresponding χ distribution. With sufficient luminosity, even this small effect could be brought to light.

It is more difficult for e^+e^- colliders to explore the $I = J = 0$ channel, but it is possible this this could be done through the reaction $\gamma\gamma \to Z^0Z^0$. In models with a low mass or weakly coupled Higgs boson, this reaction proceeds only through fermion and W boson box diagrams. Its rate is very small, of order 10^{-3} units of R. However, in models with Higgs strong interactions, the reaction can proceed by rescattering from $\gamma\gamma \to W^+W^-$, just as one finds $\gamma\gamma \to \pi^0\pi^0$ in the familiar strong interactions. The cross section for the latter process can be computed from chiral perturbation theory.[64,65] The same calculation applies to $\gamma\gamma \to Z^0Z^0$ by Goldstone boson equivalence. Including the effects of final-state interactions, one finds that the following expression for the Z^0 pair cross section:[62]

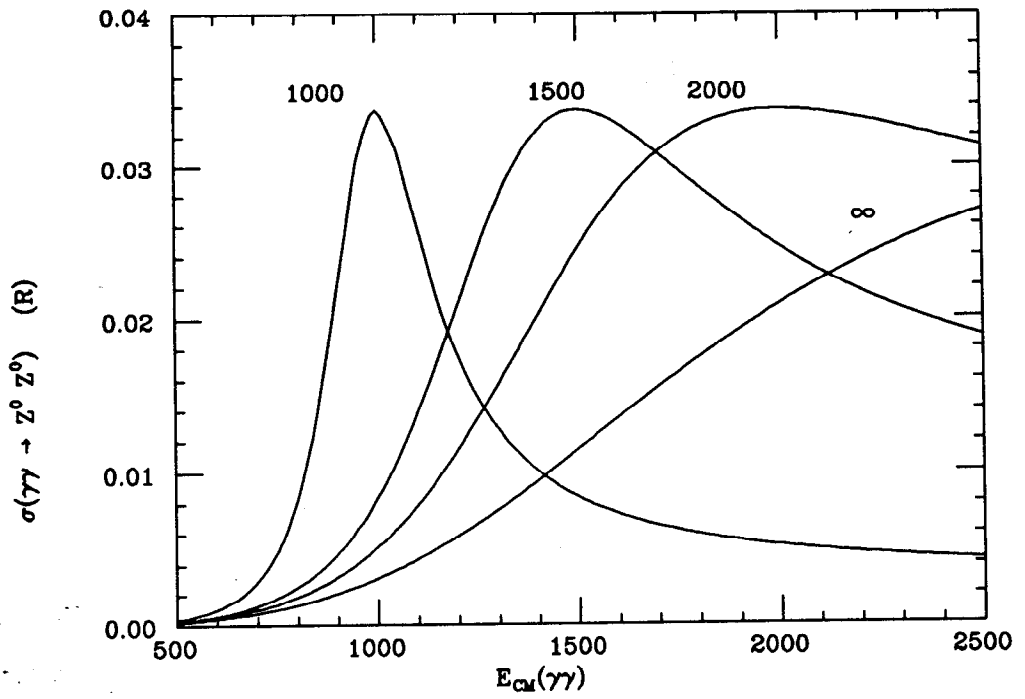

Figure 33. Total cross section for $\gamma\gamma \to Z^0Z^0$, computed using a phase shift δ_{00} with a resonance at masses of 1 TeV, 1.5 TeV, 2 TeV, ∞.

$$\sigma(\gamma\gamma \to Z^0Z^0) = \frac{1}{3\pi^2}\sin^2(\delta_{00} - \delta_{02}), \tag{27}$$

in units of R. Since chiral dynamics and explicit models predict relatively weak scattering in the 02 channel, this formula can be used to extract δ_{00}. The cross section for Z^0 pair production predicted by (27) is shown in Fig. 33 for various choices of the resonance mass M_{00}. These cross sections are small but not unreasonable for a dedicated $\gamma\gamma$ collider operating at 2 TeV in the center-of-mass.

These two experiments are not part of the program of the next linear collider, but they do belong to the program of a higher-energy machine that should evolve from it. On the other hand, the study of the strongly interacting Higgs sector is known to be one of the most difficult topics in the program of the SSC, requiring the highest luminosities and longest running periods. My discussion thus indicates that, even over the long term, e^+e^- colliders can provide interesting and significant information which complements the results from proton colliders in exploring the most deeply hidden aspects of Nature.

7. Conclusions

It is well known that an e^+e^- collider with center-of-mass energy 400–500 GeV will be able to carry out an exhaustive search for new particles and interactions in this energy region. In this article, I have explained that such a collider will also have an interesting program of physics within the standard model. The standard model makes detailed and subtle predictions for the dynamics of W and top quark pair production. I have explained how experiments at the NLC can test these predictions and use the rich structure of the standard model amplitudes to search for anomalous terms in the interactions of these particles. In particular, the ability of experiments in the NLC enviroment to reconstruct and track W bosons and to analyze their polarization opens a powerful tool for exploring their interactions and their relation to the Higgs sector. If W and t—the last and most mysterioius pieces of the standard model—hold clues to what lies beyond, those clues can be uncovered at the Next Linear Collider.

Acknowledgments

I am grateful to my colleagues in the NLC working group at SLAC, particularly Tim Barklow, David Burke, Howard Haber, Mina Petradza, Carl Schmidt, Matt Strassler, and Eran Yehudai, for helping me to shape the ideas presented here, to the participants in the Sariselka workshop, for many enlightening discussions, and to Risto Orava, Paula Eerola, Markus Nordberg, and the staff of the workshop, for providing an inspiring setting for dreams about the future of experimental particle physics.

REFERENCES

1. F. Bulos, *et. al.*, in *Proceedings of the 1982 DPF Summer Study on Elementary Particle Physics and Future Facilities (Snowmass)*, R. Donaldson, R. Gustafson, and F. Paige, eds. (Fermilab, 1982).
2. J. Ellis, in *Proceedings of the XIV International Symposium on Multparticle Dynamics*, P. Yager and J. F. Gunion, eds. (World Scientific, Singapore, 1984).
3. M. E. Peskin, in *Physics in Collision IV*, A. Seiden, ed. (Éditions Frontières, Gif, 1984).
4. *Proceedings of the Workshop on Physics at Future Accelerators (La Thuile)*, J. H. Mulvey, ed. CERN 87-07 (1987).
5. M. E. Peskin, in *Proceedings of the 15th SLAC Summer Institute*, E. Brennan, ed. SLAC-Report-328 (1988).
6. C. Ahn, *et. al.*, SLAC-Report-329 (1988).

7. *Proceedings of the First Workshop on Japan Linear Collider,* S. Kawabata, ed. KEK report 90-2 (1990); *Proceedings of the Second Workshop on Japan Linear Collider,* S. Kawabata, ed. KEK proceedings 91-10 (1991).
8. M. Chanowitz, in *Proceedings of the Second KEK Topical Conference on e^+e^- Collision Physics.* KEK proceedings (1992).
9. I. F. Ginzburg, G. L. Kotkin, V. G. Serbo, S. L. Panfil, and V. I. Telnov, *NIM,* **205,** 47 (1983), **219,** 5 (1984).
10. More complete references and discussion of the photon linear collider can be found in V. I. Telnov, these proceedings, and in D. L. Borden, D. A. Bauer, and D. O. Caldwell, SLAC-PUB-5715 (1992).
11. R. B. Palmer, *Ann. Rev. Nucl. Part. Sci.,* **40,** 529 (1990).
12. E. Yehudai, Ph. D. thesis, SLAC-report-383 (1991).
13. P. B. Wilson, SLAC-PUB-3985 (1986); R. Blankenbecler and S. D. Drell, *Phys. Rev.* **D36,** 277 (1987).
14. P. Chen and V. I. Telnov, *Phys. Rev. Lett.* **63,** 1796 (1989).
15. M. Drees and R. M. Godbole, *Phys. Rev. Lett.* **67,** 1189, (1991).
16. J. M. Cornwall, D. N. Levin, and G. Tiktopoulos, *Phys. Rev.* **D10,** 1145 (1974).
17. C. E. Vayonakis, *Lett. Nov. Cim.* **17,** 383 (1976).
18. B. W. Lee, C. Quigg, and H. Thacker, *Phys. Rev.* **D,** 1519 (1977).
19. For a pedagogical review of this theorem, see Ref. 5, Section 5.
20. J. F. Gunion, H. E. Haber, G. Kane, and S. Dawson, *The Higgs Hunter's Guide.* (Addison-Wesley, Redwood City, CA, 1990).
21. M. Davier, contribution to the Proceedings of the 1991 Lepton-Photon Symposium/EPS Conference, LAL 91-48 (1991).
22. S. L. Wu, *et. al.,* in *Proceedings of the ECFA Workshop on LEP 200,* vol. II, A. Böhm and W. Hoogland, eds. CERN 87-08 (1987).
23. See, for example, V. Barger, K. Cheung, T. Han, and D. Zeppenfeld, *Phys. Rev.* **D44,** 2701 (1991).
24. N. Cabibbo, L. Maiani, G. Parisi, and R. Petronzio, *Nucl. Phys.* **B158,** 295 (1976).
25. J. F. Gunion and H. E. Haber, contribution to the Proceedings of the 1990 DPF Summer Study, Snowmass, SCIPP-90-22 (1990).
26. A. F. Falk, M. Luke, and E. H. Simmons, *Nucl. Phys.* **B365,** 523 (1991).
27. M. B. Einhorn and J. Wudka, Santa Barbara preprint NSF-ITP-92-01 (1991).

28. A. De Rujula, M. B. Gavela, P. Hernandez, and E. Masso, CERN-TH-6272 (1991).

29. M. Claudson, E. Farhi, and R. L. Jaffe, *Phys. Rev.* **D34,** 873 (1986).

30. M. A. Samuel, G. Li, N. Sinha, R. Sinha, and M K. Sundaresan, *Phys. Rev. Lett,* **67,** 9 (1991).

31. G. L. Kane, J. Vidal, and C. P. Yuan, *Phys. Rev.* **D39,** 2617 (1989).

32. K. Hagiwara, R. D. Peccei, D. Zeppenfeld, and K. Hikasa, *Nucl. Phys.* **B282,** 253 (1987).

33. E. Yehudai, *Phys. Rev.* **D44,** 3434 (1991).

34. S. Y. Choi and F. Schrempp, *Phys. Lett.* **B272,** 149 (1991).

35. T. Barklow, these proceedings.

36. P. Roudeau, contribution to the Proceedings of the 1991 Lepton-Photon Symposium/EPS Conference, LAL 91-48 (1991).

37. W. Bartel, *et. al.*, *Phys. Lett.* **B146,** 437 (1984).

38. A similar analysis has been presented by Schaile and Zerwas, DESY–91-106 (1991).

39. M. Einhorn, D. R. T. Jones, and M. Veltman, *Nucl. Phys.* **B191,** 146 (1981).

40. F. Cavanna, D. Denegri, and T. Rodrigo, in *Proceedings of the ECFA Large Hadron Collider Workshop,* vol. II, G. Jarlskog and D. Rein, eds. CERN-90-10 (1990).

41. A. Blondel, F. M. Renard, and C. Verzegnassi, *Phys. Lett.* **B269,** 419 (1991).

42. I. Bigi, Y. Dokshitzer, V. Khoze, J. Kühn, and P. Zerwas, *Phys. Lett.* **B181,** 157 (1986).

43. I. Bigi and H. Krasemann, *Z. Phys.* **C7,** 127 (1981); J. Kühn, *Acta. Phys. Austr.* Suppl. **XXIV,** 203 (1982).

44. V. S. Fadin and V. A. Khoze, *JETP Lett.* **46,** 525 (1987), *Sov. J. Nucl. Phys.* **48,** 309 (1988).

45. These curves are computed using the prescriptions of M. E. Peskin and M. Strassler, *Phys. Rev.* **D43,** 1500 (1991).

46. R. Ruth, private communication.

47. K. Fujii, these proceedings.

48. G. L. Kane, G. A. Ladinsky, and C. P. Yuan, *Phys. Rev.* **D45,** 124 (1991).

49. C. R. Schmidt and M. E. Peskin, SLAC-PUB-5803 (1992).

50. D. Burke and M. Petradza, private communication.

51. S. Komamiya, in *Proceedings of the 1985 International Symposium on Lepton and Photon Interactions at High Energies,* M. Konuma and K. Takahashi, eds. (Kyoto University, 1986).

52. H. P. Nilles, *Phys. Repts.* **110C,** 1 (1984).

53. H. E. Haber and G. L. Kane, *Phys. Repts.* **117C,** 75 (1985).

54. H. E. Haber, these proceedings.

55. J. F. Grivaz, these proceedings.

56. R. Barbieri, in *Z Physics at LEP1,* vol. 2, G. Altarelli, R. Kleiss, and C. Verzegnassi, eds. CERN report CERN 89-08 (1989).

57. S. Dawson and G. Valencia, *Nucl. Phys.* **B352,** 27 (1991); J. Bagger, S. Dawson, and G. Valencia, FERMILAB-PUB-92-75-T (1992).

58. P. Sikivie, L. Susskind, M. Voloshin, and V. Zakharov, *Nucl. Phys.* **B173,** 189 (1980).

59. B. Mele and F. Richard, in Ref. 4, vol. II.

60. J. F. Gunion and A. Tofighi-Niaki, *Phys. Rev.* **D36,** *2671 (1987),* **D38,** 1433 (1988).

61. K. Hagiwara, J. Kanzaki, and H. Murayama, KEK-91-4 (1991).

62. C. Im and M. E. Peskin, in preparation.

63. F. Iddir, A. Le Yaouanc, L. Oliver, O. Pene, and J. C. Raynal, *Phys. Rev.* **D41,** 22 (1990).

64. J. F. Donoghue, B. R. Holstein, and Y. C. Lin, *Phys. Rev.* **D37,** 2423 (1988).

65. J. Bijnens and F. Cornet, *Nucl. Phys.* **B296,** 557 (1988).